Supporting Materials

This PDF includes:

Materials and Methods

Figs. S1 to S15.

References (1-7)

Materials and Methods

Subjects

Seven male Lister Hooded adult rats were used for the experiments. Rats were individually housed in clear plastic cages (68 cm x 44 cm x 48 cm, W x L x H) and were kept on a 12:12 hours light:dark cycle at a controlled temperature (19-23 ^{0}C) and humidity (50-70 %). The rats weighed 350-380g on the day of surgery. They were maintained on a 90% of body weight food deprivation schedule where the most recent feeding was at least 12 hours before the experiments. Water was supplied ad libitum.

Surgery and electrodes

The rats were anaesthetised with 1-3 % of isoflurane in O_2 and an 0.01mg /100g im injection of buprenorphine. They were chronically implanted in the left hemisphere with a microdrive loaded with four tetrodes (HM-L coated 90 % platinum and-10 % iridium 17 microns diameter wire). The tetrodes were tightly glued together and cut at the same level. The electrode tips were plated to reduce the impedance to 150-300 kΩ at 1 kHz. Tetrodes were aimed at the superficial layers of medial part of dorsocaudal medial entorhinal cortex (mEC) and adjacent parasubiculum (PaS) (4.3 mm lateral to the midline; 0.3 mm anterior to the sinus and 1.5 mm below the pia). Six screws were threaded into the skull and the microdrive anchored to them with dental cement. A jeweller's screw fixed to the

skull over the opposite hemisphere was used as a ground screw. After surgery the rats were given at least 7 days to recover before the experiments were started.

Histology and electrode localization

After completion of the recording sessions the rats were sacrificed using an overdose of sodium pentobarbital and perfused transcardially with saline followed by 4 % of paraformaldehyde (PFA). The brain was cryoprotected in 4 % PFA and 20 % sucrose solution and sliced into 30 micron parasagittal sections using a freezing microtome. Sections were mounted and Cresyl-Violet Nissl-stained to allow visualization of the electrode track. Recording sites were determined by measuring backwards from the deepest point of the track and ensuring that the total length of the electrode track corresponded to the amount of electrode movement as measured from the microdrive screw turns (Fig. S1). 20 % shrinkage was allowed. mEC layer II cells were identified as a densely packed strongly stained layer of cells. mEC layer III cells were less intensely stained and less densely packed. PaS superficial layers cells were identified as densely packed cells located in a dorsocaudal area above superficial layers of mEC which showed less staining and did not show a clear laminar structure.

Data Collection

Rats were allowed at least 7 days of recovery after surgery. Tetrodes were lowered 50 microns or less per day at the end of each recording session until the first cells of interest were found. Single unit data were acquired using a proprietary data acquisition system. Two infrared LEDs of different intensities and separated by 7 cm were fixed on the animal's head in order to track the animal's position and head orientation. The (x, y) coordinates of the LEDs were acquired at 50 Hz by an infrared camera attached to the ceiling above the centre of the environment.

Single cell isolation from multi-unit recordings

Isolation of single units was performed by manual cluster-cutting. Clusters were isolated in a feature space where all possible combinations of pairs of spike amplitudes recorded by four tetrodes were plotted against each other. Unit isolation was further refined by taking into account additional properties of spike waveforms such as the existence of positive pre-potentials. The quality of cluster isolation was tested by estimating the L-ratio and isolation distance(*1*) (Fig. S2). The Isolation distance shows how distant the cluster spikes are compared to other spikes recorded by the tetrode in Mahalanobis space. L-ratio indicates the amount of 'noise spikes' (i.e. spikes which are not part of the cluster) in the vicinity of the cluster. L-ratio reflects the amount of spikes that could belong to a cluster but were not included, whereas isolation distance reflects the amount of potential 'noise spikes' included into the cluster. Clusters recorded on different trials were assigned to the same cell if: a) the tetrode had not been moved between trials; b) there was minimal change in spike waveforms; c) the position of the target cluster and neighbouring clusters remained similar in feature space.

Training procedures and testing environments

The animals were recorded in a familiar square (1.3 m x 1.3 m x 0.5 m) enclosure. The sides of the wooden square enclosure were painted in light grey and the bottom in dark grey. The recording enclosure was always placed in the same position with respect to the laboratory. Distal visual cues (e.g. a white rectangular cue card, shelves, recording system etc) were available to maintain the same allocentric orientation across the trials. The animals were trained to forage for sweetened rice thrown into random locations in the enclosure approximately every 10-20 seconds. At least two 15 min trials were recorded within a day. There were 10 min intervals between every trial during which the animal rested on a holding platform located near the testing environment.

To ensure that our observations did not result from an inadequate spatial sampling resolution, for two rats (r1738 and r1739) we used a higher resolution camera (360 pixels/m) and ran longer trials (at least 30 min) in addition to the usual camera (214 pixels/m) and duration used for all the other rats. The enhanced

resolution and duration recordings did not show any differences in cell firing patterns.

In some of the sessions we also run a 10-15 min trial in which the animal foraged in a familiar 1 m diameter x 0.5 m circular enclosure.

We ran trials in the dark as well as the light but only the light trials were included in our final analysis. All the first trials of the day were excluded to minimise novelty effects.

Criteria for cell inclusion

Cells were included in the final analysis if they satisfied the following criteria: a) the animal was familiar with the testing environment: defined as having previous exposure of at least five 20 min trials recorded within at least 3 days; b) the cell was recorded for at least two trials; c) it had a spike width > 200 μs (Fig. S2); d) fired at least 100 spikes within the trial and e) had a peak firing rate > 1 Hz and a mean firing rate <5Hz (Fig. S2).

Firing rate maps

Locational firing rate map was estimated by dividing the number of spikes fired in a given part of the environment by the time spent there. Position data and spike counts were sorted into 2.5cm x 2.5cm spatial bins. Unsmoothed firing rate maps were obtained by dividing the spike count in each bin by the dwell time in that bin. The smoothed firing rate map was obtained by first applying adaptive smoothing (see 'Adaptive Smoothing') to the dwell time and spike maps and then dividing them. Color bars represent firing rate in deciles of the range of firing rates (top 10 % in red, bottom 10 % in blue). Unvisited bins are shown in white.
Directional firing rate was estimated by dividing spike counts and dwell time into 3 degree bins). Adaptive smoothing was applied to spike and dwell time maps before dividing them.

Adaptive smoothing

Adaptive smoothing(*2*) was applied to the firing rate maps. In brief, to calculate the firing rate for a given bin the number of spikes assigned to that bin is defined by a circle centred at the bin with the radius r. The radius of the circle is expanded until

$$r \geq \frac{\alpha}{n\sqrt{s}} \tag{1}$$

where $\alpha = 5000$, n is the number of bins and s is the number of spikes lying within the circle.

Criteria for cell classification

All cell types were identified by comparing a relevant measure to a threshold value calculated as the 95th percentile value of shuffled data (Fig. S3). The data was shuffled(*3*) by wrapping the time-shifted spike train around the position data. The spike train was shifted by a random duration more than 20 s and less than trial duration minus 20s. Cells were classified as spatially periodic based on the maximum power of their two dimensional Fourier spectrogram; cells were classified as grid cells based on their gridness score; cells were classified as directional cells based on the length of their Rayleigh vector. The shuffling was performed on all cells, on a cell-by-cell basis, until the 95th percentile of the maximum power Fourier component converged to a constant.

Identifying cells with a spatially periodic firing pattern

To estimate the degree of periodic regularity in the spatial distribution of cell firing we calculated the two-dimensional Fourier spectrogram:

$$F\left[l_y, l_x\right] = \frac{1}{fr_{mean}\sqrt{M_x N_y}} \sum_{n=0}^{N-1} \sum_{m=0}^{M-1} f\left[m,n\right] e^{-2\pi i\left(\frac{ml_y}{M} + \frac{nl_x}{N}\right)} \tag{2}$$

where $i = \sqrt{-1}$, and $f[m,n]$ is the unsmoothed firing rate map, with mean firing rate subtracted, zero-padded to have size $M_x \times N_y = 256 \times 256$ to increase the spatial resolution of the Fourier spectrogram. The spectrogram is a matrix of Fourier coefficients corresponding to a basis set of plane waves of varying wavelength and orientation (Fig. 1F). Each plane wave is specified by the integer values (l_y, l_x) which identify the y and x components of the wave vector in terms of the number of spatial cycles covering the entire firing rate map along its height and its width respectively (see equation 6, below). fr_{mean} is the mean firing rate (the total number of spikes divided by trial duration). M_x and N_y are the width and length in bins of the original firing rate map before zero-padding. Division by $\sqrt{M_x N_y}$ enables comparison of Fourier power between firing rate maps from different size environments. Normalising by mean firing rate enables comparison of cells with different firing rates.

The power of the Fourier spectrum is calculated as

$$P[l_y, l_x] = \sqrt{F_r^2[l_y, l_x] + F_i^2[l_y, l_x]} \qquad (3)$$

where F_r and F_i are the real and the imaginary parts of Fourier spectrum respectively.

The maximum Fourier power $P[l_x, l_y]$ of the firing pattern was used to assess the degree of its spatial periodicity.

Estimating and displaying spatial periodicity

We used the shift property of two-dimensional Fourier spectrograms to shift low frequencies to the centre and high frequencies to the periphery of the Fourier spectrogram by changing the signs of all points in the rate map $f[m,n]$:

$$f'[m,n] = f[m,n](-1)^{m+n} \qquad (5)$$

and applied equations (2) and (3) to $f'[m,n]$ to obtain the centred Fourier spectrogram. The wave vector corresponding to point (l_y, l_x) in the spectrogram is:

$$k_y = \frac{2\pi\left(l_y - l_{cy}\right)}{Mb}; \qquad k_x = \frac{2\pi\left(l_x - l_{xc}\right)}{Nb} \tag{6}$$

where $\left(l_{cy}, l_{cx}\right)$ is the coordinate of the centre of the spectrogram, and b is the bin size in meters. The corresponding spatial wavelengths are:

$$\lambda_y = \frac{2\pi}{k_y}; \qquad \lambda_x = \frac{2\pi}{k_x}. \tag{7}$$

The overall wavelength is:

$$\lambda = \sqrt{\lambda_x^2 + \lambda_y^2} \tag{8}$$

and the direction of the wave vector is

$$\varphi = \operatorname{atan}\left(\frac{k_y}{k_x}\right). \tag{9}$$

Hence the direction of the orientation of the periodic bands is:

$$\theta = \varphi + 90^{\circ} \tag{10}$$

Estimating the degree of spatial regularity with random field shuffling using Voronoi segmentation

To estimate the degree of spatial periodicity of the firing map pattern of spatially periodic cells compared to the degree of periodicity expected by chance if the fields were randomly distributed across the environment, we applied Voronoi algorithm(*4*) to segment the environment into the number of parts approximately equal to the number of the firing fields (Fig. S4 A-B) taking all local maxima of the smoothed rate map (see 'Adaptive Smoothing') as the centres of the Voronoi polygons. The polygons were randomly rotated from 0 to 360 degrees and random coordinates (from zero to the side length of the square environment) were assigned to the centres of Voronoi polygons – the truncation of the fields near the edges was permitted (Fig. S4C-F). In case the polygons overlapped, the newest value was

assigned to the bin. Bins from the polygons which escaped the 'virtual arena' were stored (further called 'the truncated bins'). The truncated bins and the bins from the edges of the Voronoi polygons of the original cell firing map were randomly assigned to the empty bins in a virtual arena. The two dimensional Fourier spectrograms of the surrogate firing map was calculated and divided by its mean firing rate to compensate for any loss in Fourier power due to the loss of overlapping bins. The maximum Fourier power was stored. The procedure was repeated for repeated 50 times and 95^{th} percentile of the surrogate power value was taken as the threshold for the regularity significantly larger than expected by chance.

Displaying the polar distribution of Fourier power

To study the distribution of Fourier power over orientations it was convenient to display the two dimensional Fourier spectrogram as a polar plot, referred to as a Fourier polar plot (Fig. S5). In this plot the mean power from all wavelengths at a given orientation was calculated for all orientations, smoothed using a Gaussian kernel with width 17 degrees (standard deviation = 13 degrees).

Defining significant Fourier components of spatially periodic cells

We estimated the presence of significant plane-wave Fourier components in the two dimensional Fourier spectrograms as follows. To reduce effects of noise the 50^{th} percentile value of power in shuffled data was subtracted from the two dimensional Fourier spectrogram and negative values set to zero. To exclude spatial sub-harmonics significant components had to be larger than 10% of the maximum power in the polar Fourier spectrogram (obtained from the two dimensional Fourier spectrogram after removal of the 50^{th} percentile shuffled power value). Significant peaks with orientations within 10 degrees of a higher peak were ignored to rule out local maxima. Around 6% of the spatially periodic cells had more than 4 components (not shown in Figs. 1,3) and were not included into the final analysis, since most of the time they resulted from an error in estimating the number of components (e.g. the sub-harmonic frequencies were included etc). All of the spatially periodic cells with all of their components are shown in Fig.S15.

The wavelength distribution of all significant Fourier components

The wavelength of a significant Fourier component was calculated by first obtaining its orientation from the polar Fourier spectrogram and then making a 'line mask' aligned along this orientation in the two dimensional Fourier spectrogram (i.e. only the Fourier power laying along the orientation and starting on the centre of the spectrogram were taken into account). The maximum point on the mask was taken as the wavelength.

The wavelength clustering of all significant Fourier components

To evaluate how clustered the wavelengths are we applied k-means clustering of the wavelengths of all the significant spatial components for each animal (nonGCs and GCs were combined). The number of k clusters was chosen from 2 to 4 (judging by eye from the Fig. S7). The tightness of the k clusters was evaluated by calculating the standard deviation of the points in the cluster and comparing it to the 95^{th} percentile of the smallest standard deviation of the randomly shuffled points (the number of point shuffled was equal to the number of data points and the number of k clusters applied on the surrogate data was the same as applied on the real data). The clusters with the wavelengths comparable to the side length of the square environment were not evaluated since these wavelengths would show more variability due to the sampling limitations (Nyquist sampling theorem, wavelengths larger than half of the environment cannot be sampled precisely).

Distribution of orientations of the significant Fourier components

The distribution of the orientations of all the significant Fourier components of spatially periodic cells was obtained and smoothed using 17 degrees Gaussian kernel (with 13 degree standard deviation).

Assessing* 60^o *clustering of the absolute and relative orientations of Fourier components

To test for clustering of the orientations of the significant Fourier components of the grid cells within an animal at multiples of 60^o, we found the distribution of orientations modulo 60^o and mapped this onto 360^o (i.e. orientation θ became 360(θ mod 60)/60). We then calculated the Rayleigh vector R to assess the extent of uni-modal clustering at this modulo angle.
A similar procedure was used to test for 60^o clustering of the relative orientations of neighbouring Fourier components (Fig. 3H).

Stability of the rate map and Fourier-components of spatially periodic cells

To estimate the inter-session and inter-day stability respectively we calculated the Pearson product-moment correlation coefficient between the rate maps of two consequent trials within the same day and between the rate maps of the first available trials across two consequent recording.

In addition, to evaluate the stability of the orientations of significant Fourier components we calculated the Pearson product-moment correlation coefficient between the Fourier polar plots. Unlike the stability measure obtained from rate maps, this stability measure is not sensitive to the changes in firing rates of individual fields or to translations of the firing pattern.

Identifying grid cells

Gridness was obtained as in (5). We calculated the spatial autocorrelogram as

$$r\left(\tau_x,\tau_y\right)=\frac{n\sum f\left(x,y\right)f\left(x-\tau_x,y-\tau_y\right)-\sum f\left(x,y\right)\sum f\left(x-\tau_x,y-\tau_y\right)}{\sqrt{n\sum f\left(x,y\right)^2-\left(\sum f\left(x,y\right)\right)^2}\sqrt{n\sum f\left(x-\tau_x,y-\tau_y\right)^2-\left(\sum f\left(x-\tau_x,y-\tau_y\right)\right)^2}}$$

(4)

where $r(\tau_x, \tau_y)$ the autocorrelation between bins with spatial offset τ_x and τ_y. f is the firing rate map of the cell with no smoothing applied; *n* is the number of overlapping bins in two offset copies of the map. The autocorrelogram was smoothed using a two-dimensional Gaussian kernel of 5 bins with standard deviation equal to 2 bins. The six local peaks of the autocorrelogram were defined as the six local maxima with $r > 0$ closest to the central peak (excluding the central peak itself). Gridness was calculated by defining a mask on the spatial autocorrelogram centred on the central peak but excluding the peak itself bounded by a circle defined by the mean distance from the centre to the closest peaks multiplied by 2.5. This area was rotated in 30 degrees increments up to 150 degrees and for each rotation the Pearson product-moment correlation coefficient was calculated against the un-rotated mask. Gridness is then calculated taking the difference between the minimum correlation coefficient for rotations of 60 and 120 degrees and the maximum correlation coefficient for rotations of 30, 90 and 150 degrees.

Identifying directional modulation of cell firing

The uni-modal directionality of cell firing was evaluated using the Rayleigh vector, i.e. the length of the mean resultant vector calculated from the binned and smoothed polar rate map.

Calculating time-windowed spatial autocorrelograms

The standard spatial autocorrelogram represents the probability of pairs of spikes occurring with a specific displacement (x,y) displayed as a function of (x,y), calculated over locational bins to allow normalisation by dwell time. Time-windowed spatial autocorrelograms represent the same information, but restricted to pairs of spikes fired within a specific time of each other. We calculated the gridness score of spatially periodic cells from the time-windowed spatial autocorrelogram in the normal way (using the 'ring mask' obtained from the whole trial spatial autocorrelogram, see above), and examined how it changes as we increase the duration of the sliding time-window (Fig. S13).

Estimating theta modulation of cell firing

The degree of theta modulation was estimated by obtaining the unsmoothed temporal autocorrelogram of the cell's spike train for time delays ranging from 1 to 500 ms with a bin size of 1ms. The autocorrelogram was zero-padded from 500 bins to 2^{13} bins to enhance the temporal resolution of the one-dimensional Fourier spectrogram. Similar to criteria described previously(*3, 6, 7*), a cell was considered theta modulated if the mean power within 1 Hz of the peak in the 6-10 Hz range was at least 4 times greater than the mean power in the 2-125 Hz range.

References

1. N. Schmitzer-Torbert, J. Jackson, D. Henze, K. Harris, A. D. Redish, Quantitative measures of cluster quality for use in extracellular recordings, *Neuroscience* **131**, 1–11 (2005).

2. W. E. Skaggs, B. L. McNaughton, K. M. Gothard, E. J. Markus, An Information-Theoretic Approach to Deciphering the Hippocampal Code, *IN* **5**, 1030–1037 (1993).

3. T. J. Wills, F. Cacucci, N. Burgess, J. O'Keefe, Development of the Hippocampal Cognitive Map in Preweanling Rats, *Science* **328**, 1573–1576 (2010).

4. G. Voronoi, Nouvelles applications des paramètres continus à la théorie des formes quadratiques, *Journal für die Reine und Angewandte Mathematik* **133**, 97–178 (1908).

5. T. Hafting, M. Fyhn, S. Molden, M.-B. Moser, E. I. Moser, Microstructure of a spatial map in the entorhinal cortex, *Nature* **436**, 801–806 (2005).

6. C. N. Boccara *et al.*, Grid cells in pre- and parasubiculum, *Nat Neurosci* **13**, 987–994 (2010).

7. R. F. Langston *et al.*, Development of the Spatial Representation System in the Rat, *Science* **328**, 1576–1580 (2010).

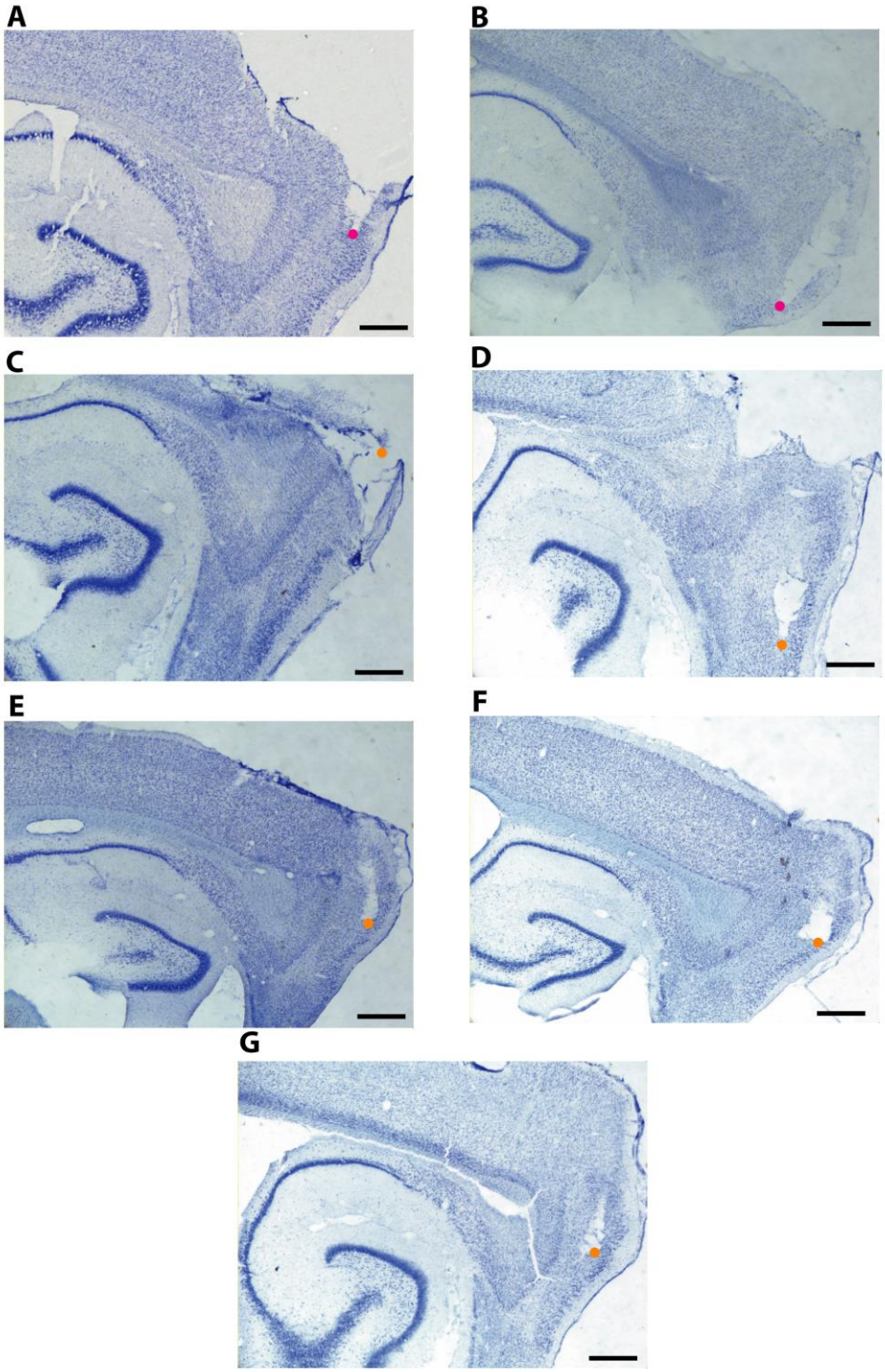

Fig. S1. Seven sagittal Nissl-stained brain sections showing the recording locations in superficial layers II-III in PaS, (**A-B**) magenta, and in mEC, (**C-G**) orange. Scale bar indicates 500µm**.** (**A**: r1682; **B**:r1738; **C**:r1728; **D**: r1709; **E**: r1737; **F**:r1739; **G**:r1710)

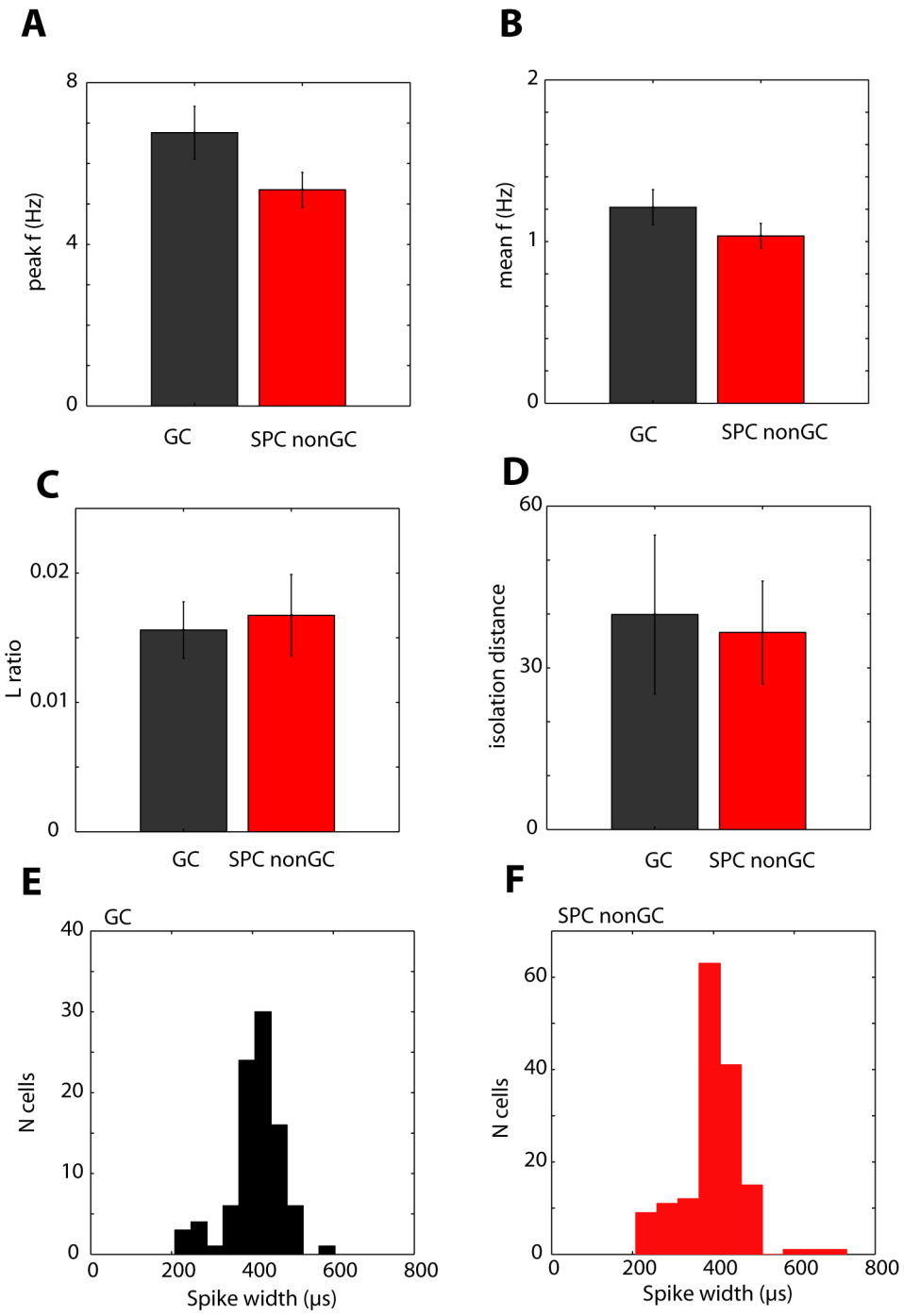

Fig. S2. Firing properties and cluster quality of spatially periodic non-grid cells (red) are comparable to grid cells (black), P>0.05. (**A-B**) Peak, a, and mean, b, firing rates averaged across all the rats. (**C-D**), L ratio, (C), and isolation distance, (D), averaged across all the rats. (**E-F**) Distribution of spike width (peak-trough) of grid cells and other spatially periodic cells. The average spike width is around 400 μs independent of the recording site.

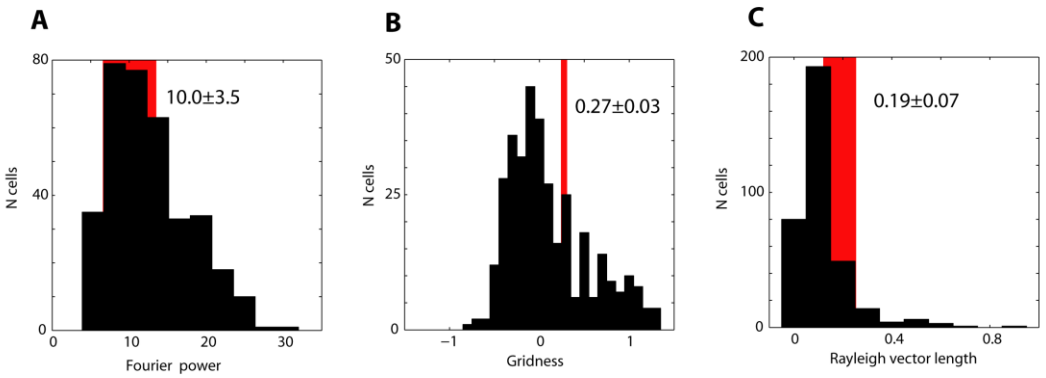

Fig. S3. Frequency histograms of maximum normalised Fourier power, (**A**), gridness, (**B**), and Rayleigh vector length, (**C**). Red bars represent the range of 95th percentile values from shuffled data. The range is defined as mean threshold ± standard deviation.

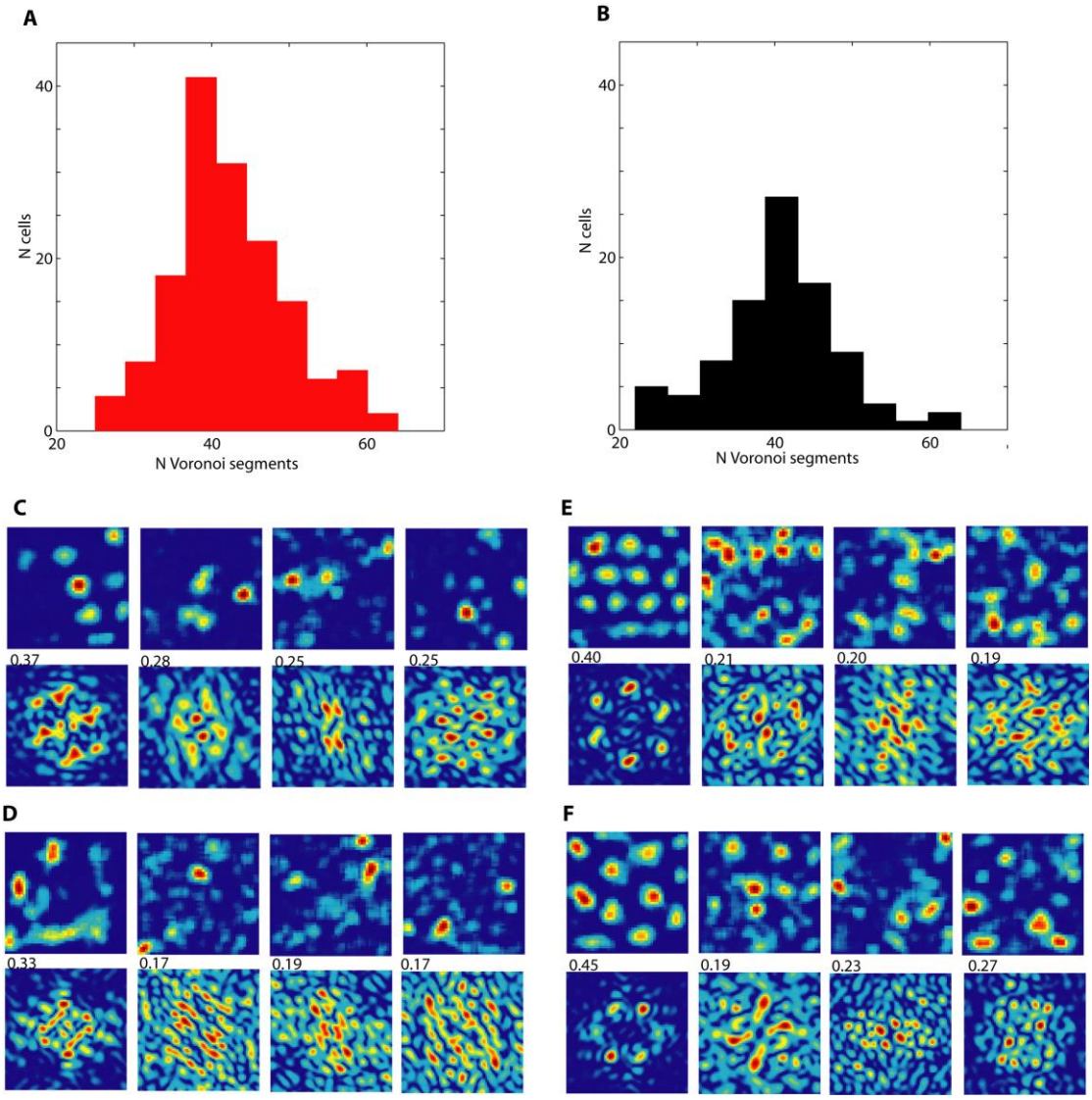

Fig. S4. Distribution of the number of Voronoi segments of spatially periodic non-grid cells, **(A)**, and grid cells, **(B)**. **(C-D)** two examples of spatially periodic non-grid cell rate maps and their 2D Fourier spectrograms, most left column. The remaining three columns show examples of their rate map surrogates with randomly shuffled Voronoi segments. **(E-F)** two examples of grid cell rate maps and their 2D Fourier spectrograms, most left column. The remaining three columns show examples of their rate map surrogates with randomly shuffled Voronoi segments. The number of Voronoi segments is 33 in (C), 36 in (D), 33 in (E) and 26 in (F). The gridness score is -0.41 in (C), -0.07 in (D), 0.88 in (E) and 0.82 in (F).

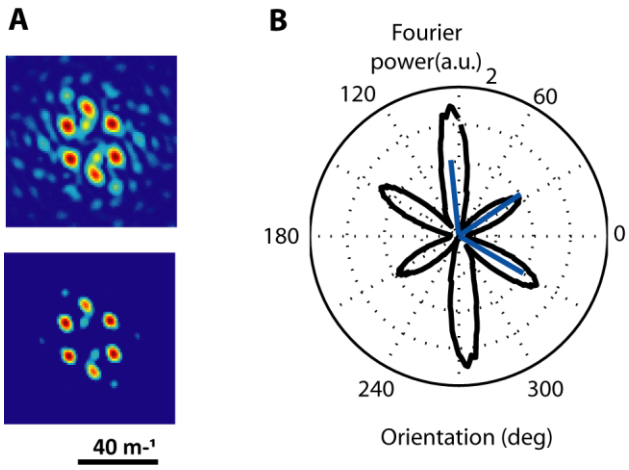

Fig. S5. Estimating significant Fourier components from Fourier polar plots. (**A**) A typical 2D Fourier spectrogram of a grid cell before subtraction of 50th percentile value from shuffled data (top) and after (bottom). (**B**) Fourier polar plot calculated from the 'cleaned' two dimensional Fourier spectrogram in a, bottom; values smaller than 10% of the maximum power of the Fourier polar plot were removed to avoid counting sub-harmonics. Orientations of the significant Fourier components are shown in blue.

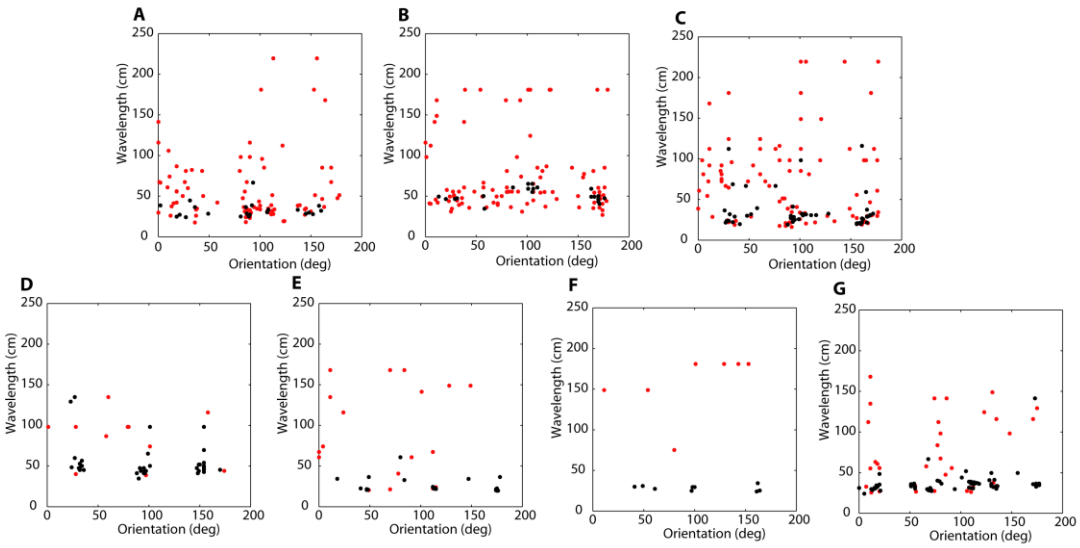

Fig. S6. The distributions of wavelengths and orientations of significant Fourier components. (**A-B**) cells from PaS; (**C-G**) cells from mEC. ((**A**): r1682; (**B**) : r1738; (**C**): r1728; (**D**): r1709; (**E**): r1737; (F):r1739; (**G**): r1710). Grid cells shown in black, other spatially periodic (non-grid) cells shown in red.

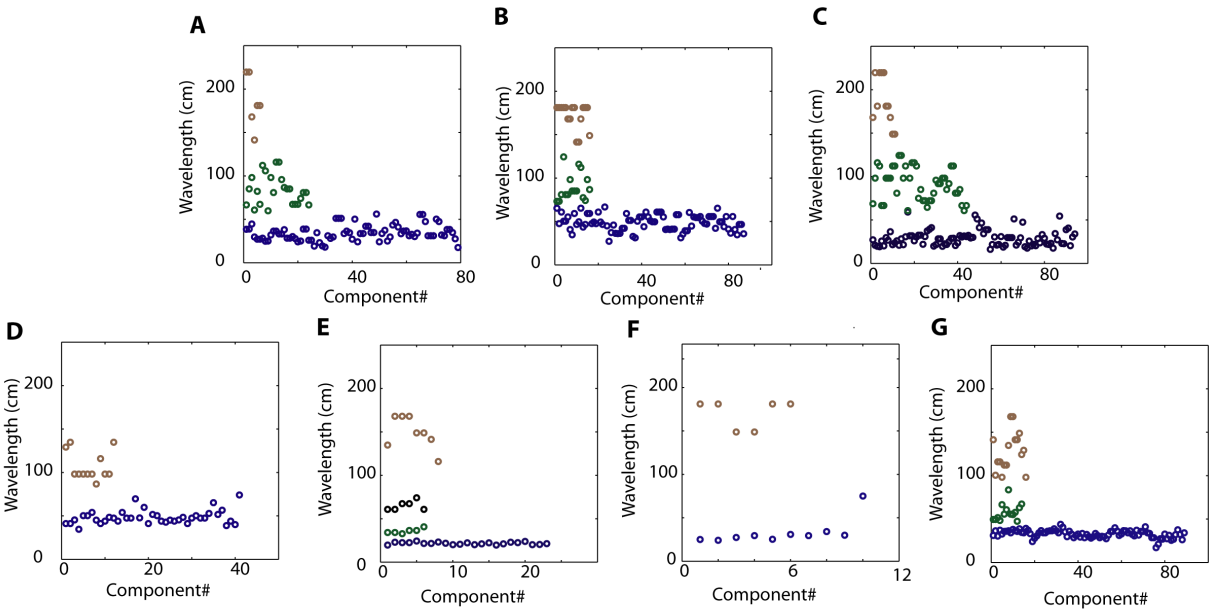

Fig. S7. The clusterization of wavelengths of significant Fourier components. Different colours mark distinct clusters. Brown clusters corresponding to the larger wavelengths (with mean wavelength >100 cm) were not included into the analysis. (**A-B**) cells in PaS; (**C-G**) cells in mEC (**A**: r1682; **B**: r1738; **C**: r1728; **D**: r1709; **E**: r1737; **F**: r1739; **G**: r1710. All clusters were significantly more clustered than expected by chance (P<0.05). Namely, A: blue: 34.4+8.9(<17.5), green: 83.6+17.3(<19.4); B: blue: 48.6+9.1(17.7); green: 89.5+15.9 (16.5); C: blue: 28.9+9.0 (<19.8); green: 91.0+18.8 (<20.2); D: blue: 48.4+7.9(<14.3); E: 21.7+1.3(<8.6); green: 35.9+2.8(<10.6); black: 65.2+5.4(10.9); F: blue: 33.1+15.1(<18.0); G: blue: 33.0+4.5(<13.6); green: 58.0+9.8(<14.1), here the mean+sd of the data was specified (and compared to the 95th percentile of sd of the data surrogate).

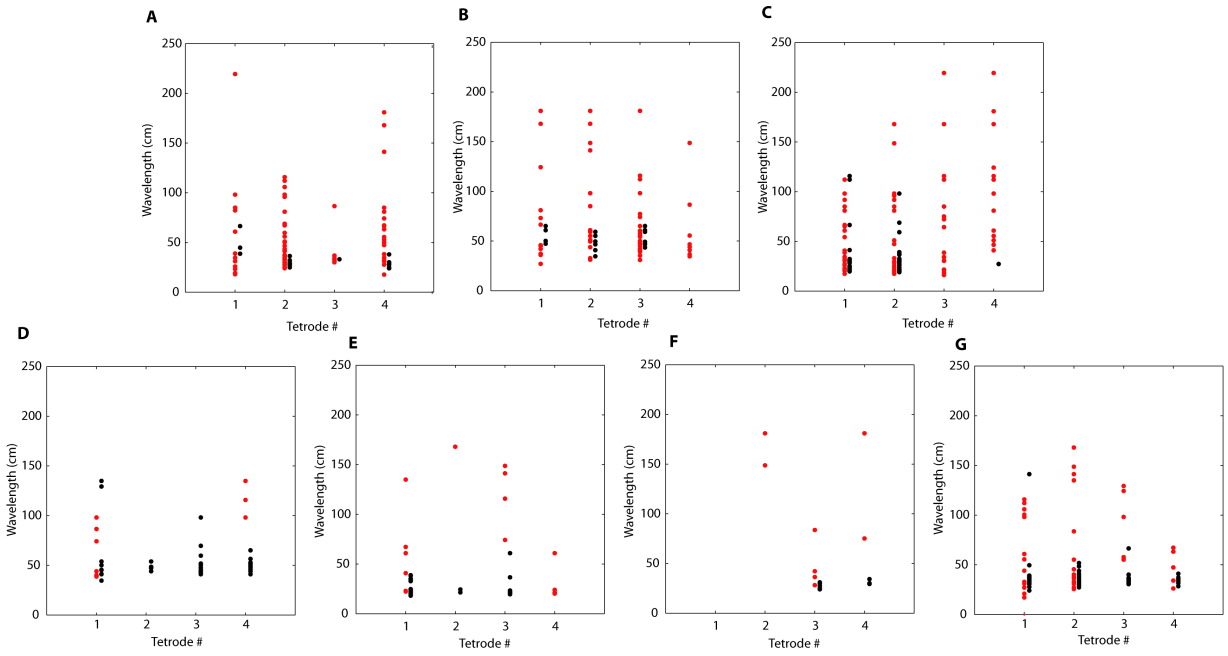

Fig. S8. The distributions of wavelengths of significant Fourier components for each tetrode in each animal. (**A-B**) cells from PaS; (**C-G**) cells from mEC. ((**A**): r1682; (**B**) : r1738; (**C**): r1728; (**D**): r1709; (**E**): r1737; (F):r1739; (**G**): r1710). Grid cells shown in black, other spatially periodic (non-grid) cells shown in red.

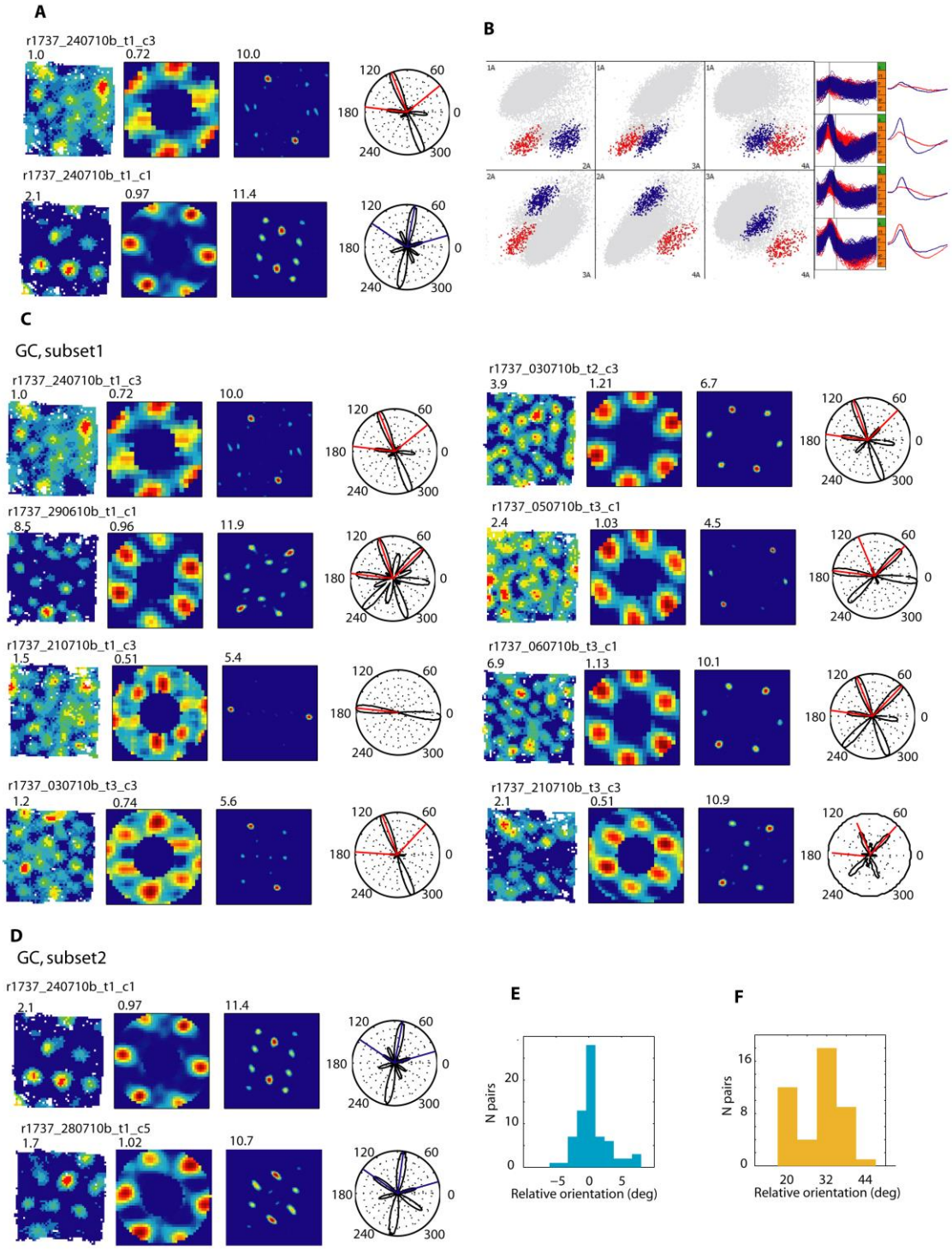

Fig. S9. Two distinct subsets of grid cells of different scale and orientation recorded from the same animal (r1737). (**A**) Two simultaneously recorded grid cells of different scale and orientation. (**B**) Clusters and waveforms of cells in a; cell1 in blue, cell3 in red. (**C**) All grid cells from subset1 (sharing scale and orientation with cell1); (**D**) all grid cells from subset2 (sharing scale and orientation with cell2). (**E**) Difference in orientation of the same component for cells within each subset. The mean difference equal to 0.74^0 (t_{69}=-0.04^0; P=0.97). (**F**) Difference in orientation between corresponding components between subsets. The mean difference is equal to 30.6^0 (t43=-0.01^0; P=0.99).

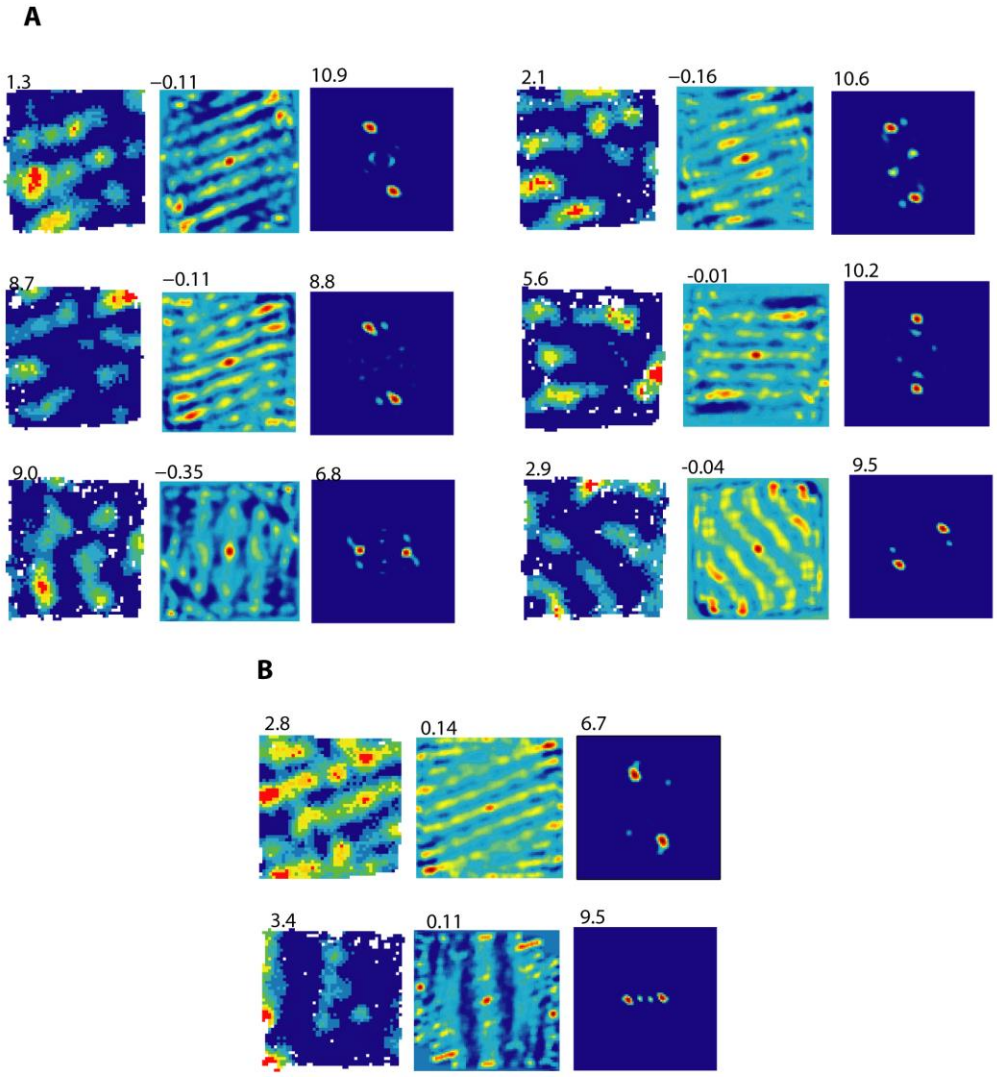

Fig. S10. Examples of band-like cells in PaS, (**A**), and in mEC, (**B**). The rate map (1.3x1.3m^2 enclosure), spatial autocorrelogram and 2D Fourier spectrogram with peak firing rate, gridness and maximum Fourier power indicated (top left) are shown for each cell.

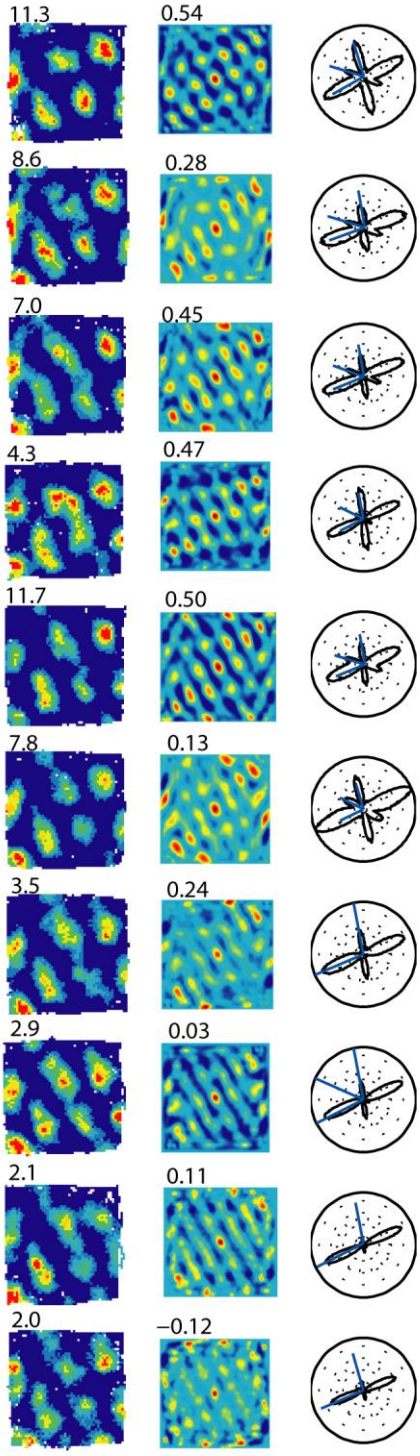

Fig. S11. Ten trials of the same spatially periodic cell recorded across five days. Rate maps with the peak firing rates, left, spatial autocorrelograms with the gridness score, middle, and Fourier polar plots, right, are shown. The significant Fourier components are indicated in blue.

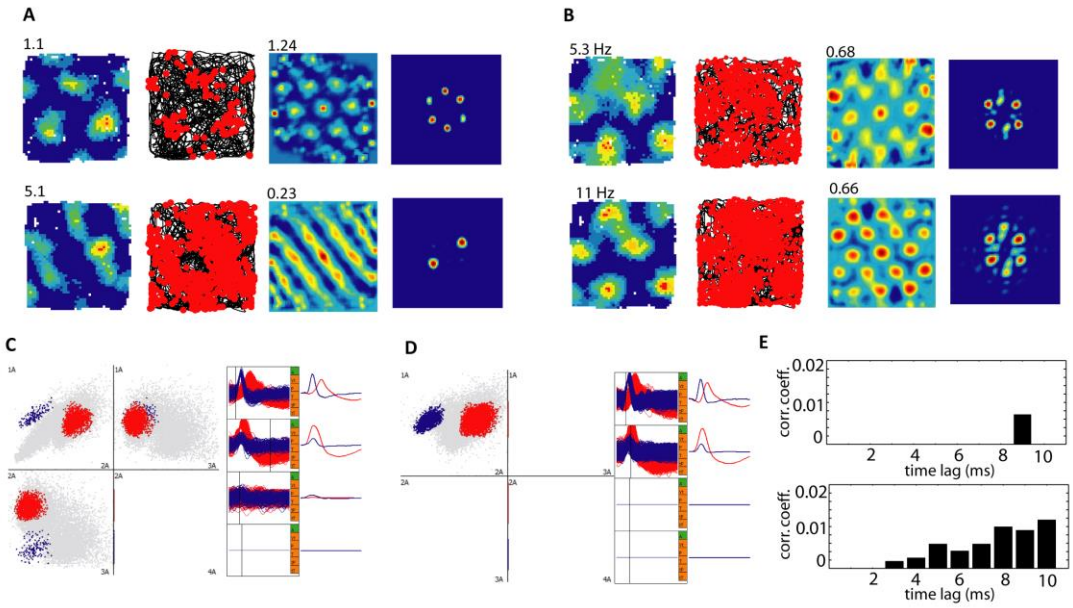

Fig. S12. Grid cell changing into a band-like cell. (**A**) Rate map, spikes overlaid on the path, spatial autocorrelogram and 2D Fourier spectrogram of a grid cell recorded on the first and second days ((A), top & bottom rows, respectively); corresponding cluster and spike waveforms shown in blue in (**C**) & (**D**)). (**B**) Similar plots for a simultaneously recorded neighbouring grid cell on the first and second days ((B) top & bottom rows respectively). Its cluster and spike waveforms shown in red, (C) & (D). The similarity of waveforms from one day to another of both of the cells and the similarity of firing pattern of the grid cell in (B) strongly suggest that the blue cluster in ((C), first day) and ((D) second day) correspond to the same cell. The third tetrode channel was lost on the second day of the recordings. (E) temporal autocorrelogram of the grid cell in (A) during the first trial, top, and the second trial, bottom.

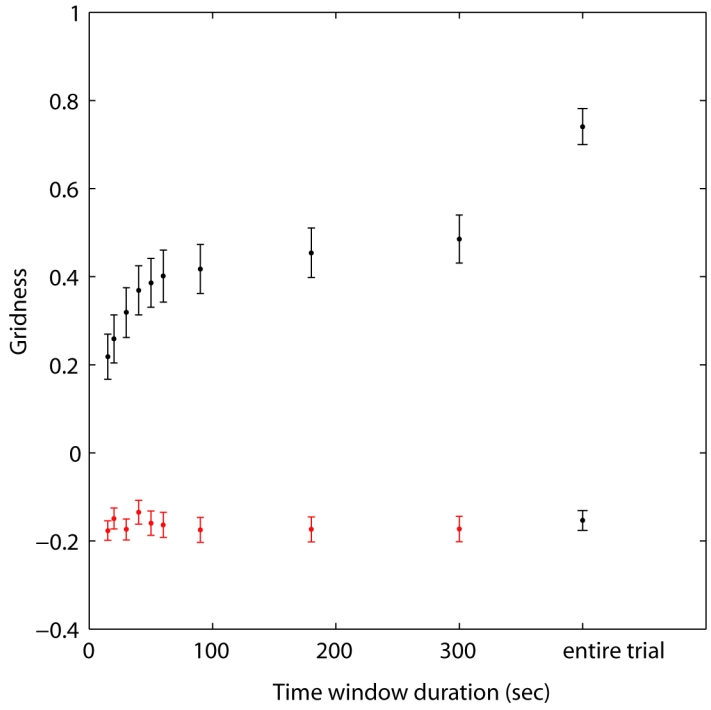

Fig. S13. The gridness of time windowed spatial autocorrelograms of grid cells (black) and other spatially periodic cells (red). The time windows used were: 15, 20, 30, 40, 50, 60, 90, 180, 300s. The minimum number of spikes per trial was 600. Notice that the grid scores of spatially periodic non-grid cells (red) do not increase with shorter time windows indicating that they are not temporally drifting grid patterns.

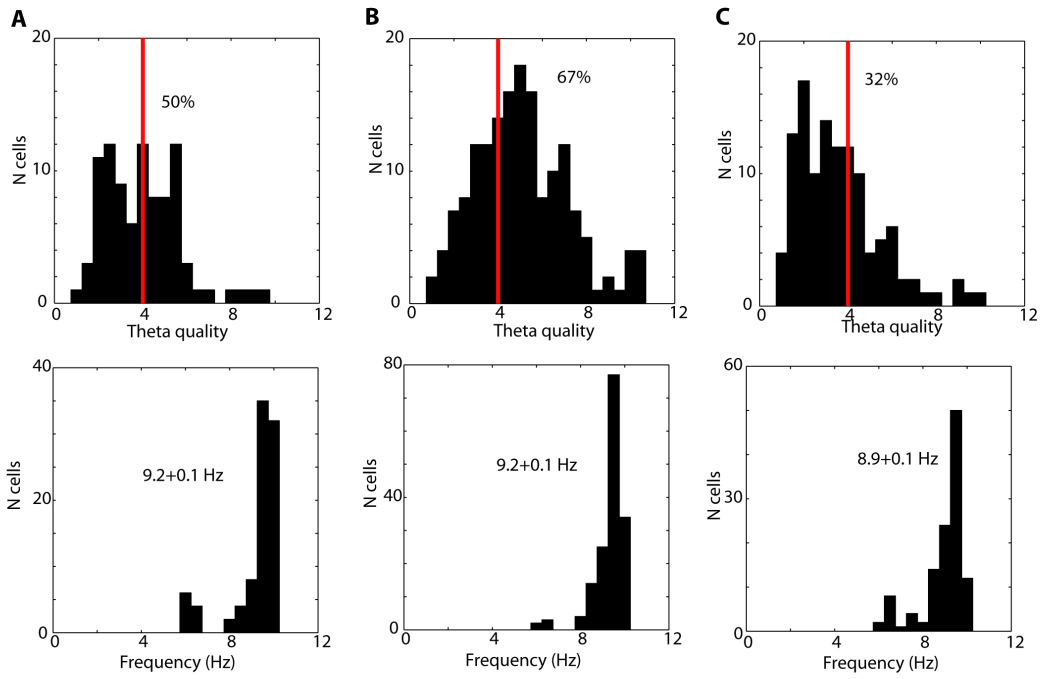

Fig. S14. Theta modulation of the firing of spatially periodic cells (SPCs) and non-SPCs. Cells were defined as theta modulated, if their θ score exceeded 4 (shown in red). (**A**) 50% of grid cells were theta modulated with mean frequency 9.2±0.1 Hz (bottom). (**B**) 67% of non-grid cell SPCs were theta modulated with mean frequency 9.2±0.1 Hz. (**C**) 32% of non-SPCs were theta modulated with mean frequency 8.9±0.1 Hz (bottom).

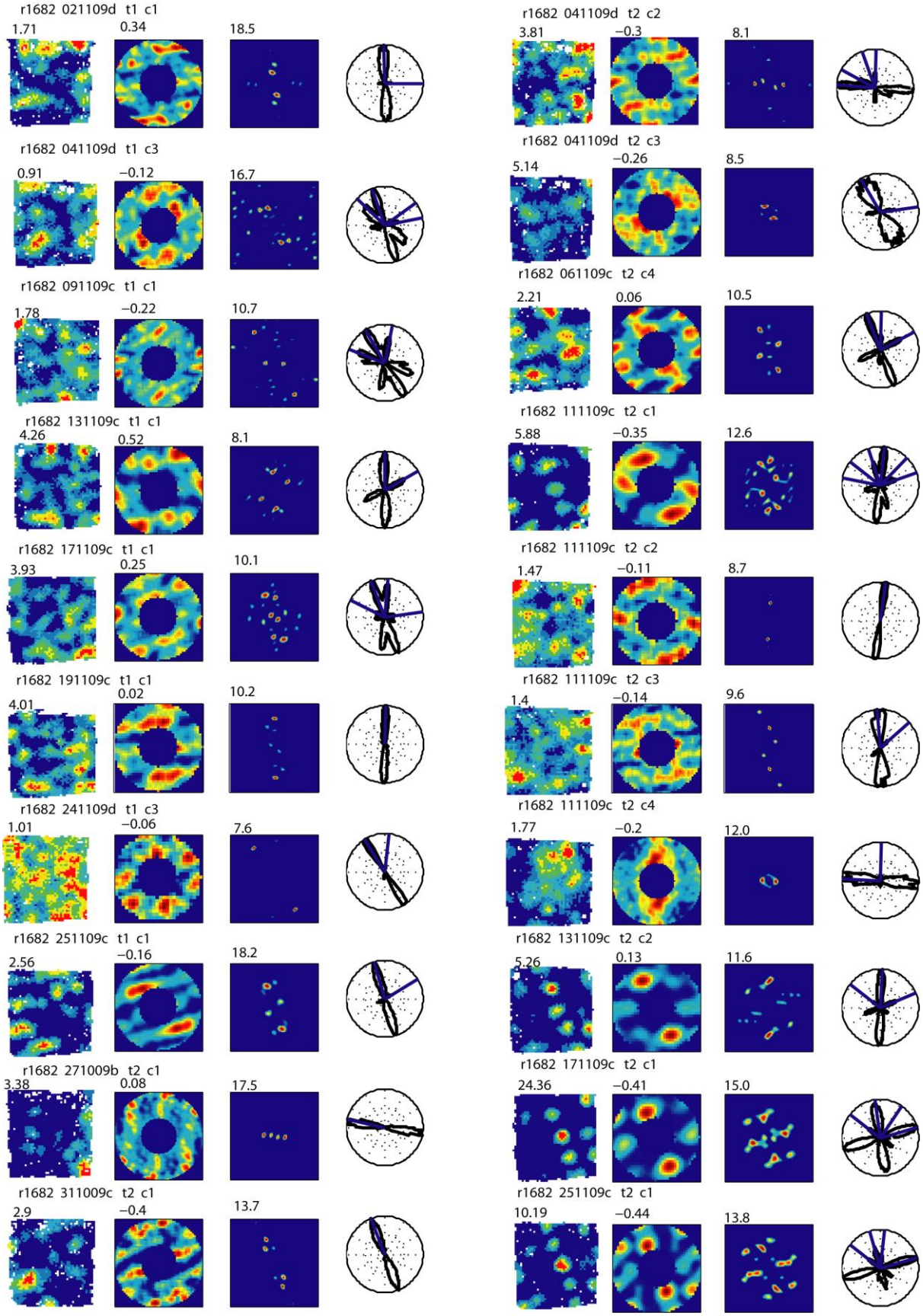
r1682 021109d t1 c1
1.71
0.34
18.5
r1682 041109d t1 c3
0.91
−0.12
16.7
r1682 091109c t1 c1
1.78
−0.22
10.7
r1682 131109c t1 c1
4.26
0.52
8.1
r1682 171109c t1 c1
3.93
0.25
10.1
r1682 191109c t1 c1
4.01
0.02
10.2
r1682 241109d t1 c3
1.01
−0.06
7.6
r1682 251109c t1 c1
2.56
−0.16
18.2
r1682 271009b t2 c1
3.38
0.08
17.5
r1682 311009c t2 c1
2.9
−0.4
13.7
r1682 041109d t2 c2
3.81
−0.3
8.1
r1682 041109d t2 c3
5.14
−0.26
8.5
r1682 061109c t2 c4
2.21
0.06
10.5
r1682 111109c t2 c1
5.88
−0.35
12.6
r1682 111109c t2 c2
1.47
−0.11
8.7
r1682 111109c t2 c3
1.4
−0.14
9.6
r1682 111109c t2 c4
1.77
−0.2
12.0
r1682 131109c t2 c2
5.26
0.13
11.6
r1682 171109c t2 c1
24.36
−0.41
15.0
r1682 251109c t2 c1
10.19
−0.44
13.8

r1682 251109c t2 c3

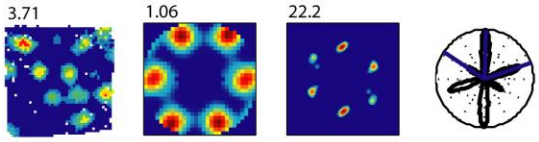

r1682 261109c t2 c1

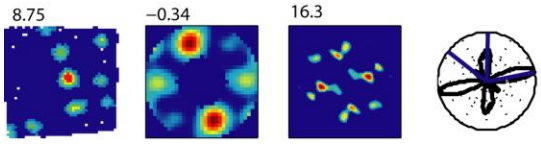

r1682 261109c t2 c3

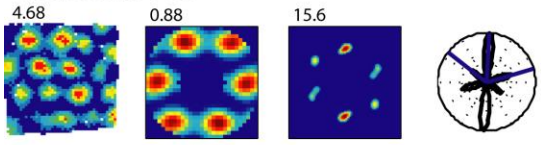

r1682 271109b t2 c1

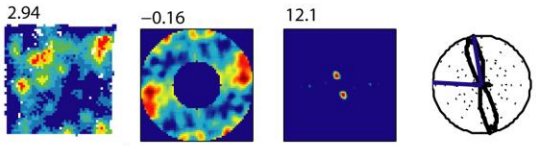

r1682 271109b t2 c3

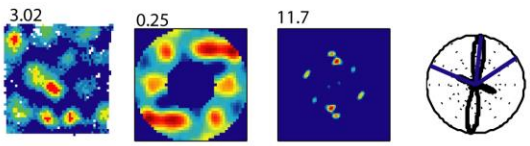

r1682 301109b t2 c3

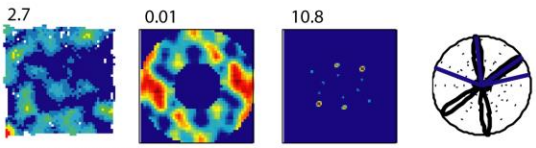

r1682 301009b t3 c1

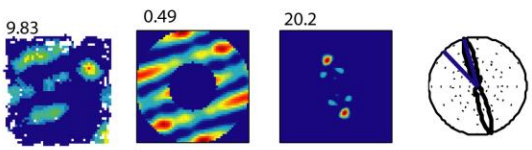

r1682 021109d t3 c1

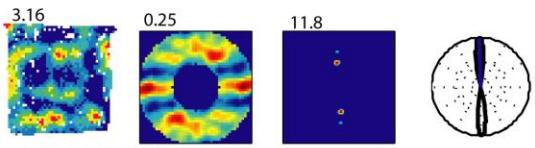

r1682 041109d t3 c1

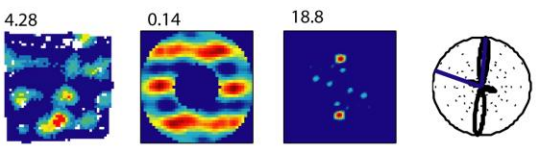

r1682 041109d t3 c2

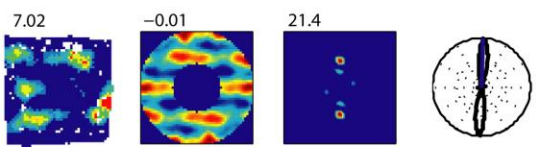

r1682 171109c t3 c1

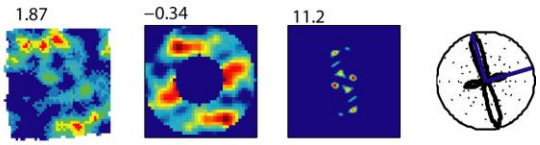

r1682 171109c t3 c3

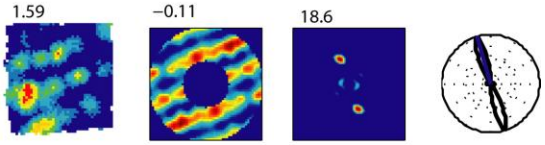

r1682 041109d t4 c2

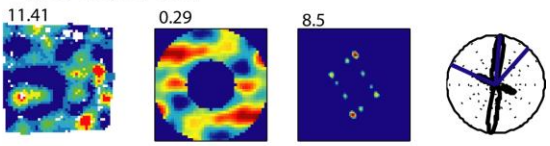

r1682 061109c t4 c4

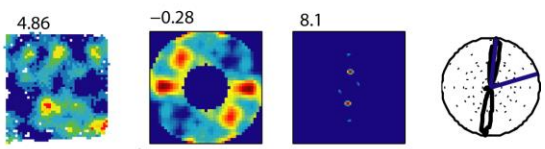

r1682 101109d t4 c1

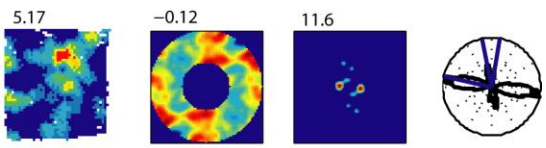

r1682 131109c t4 c1

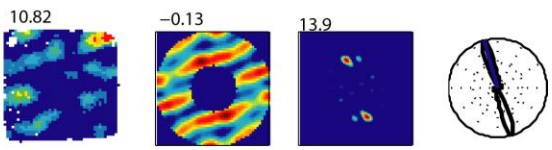

r1682 171109c t4 c1

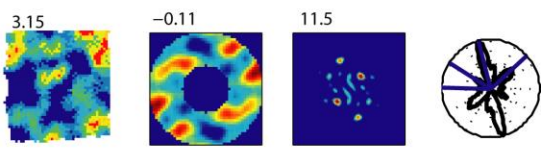

r1682 171109c t4 c2

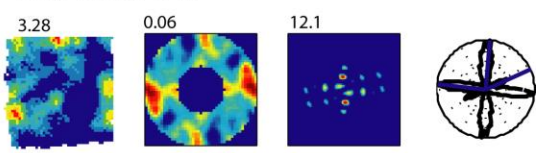

r1682 171109c t4 c7

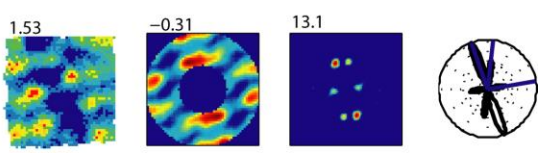

r1682 241109d t4 c1

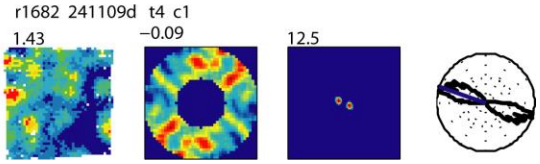

r1682 241109d t4 c3

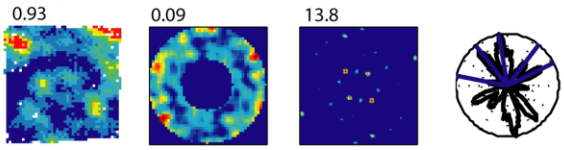

r1682 271109b t4 c3

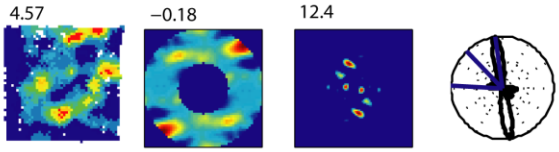

r1682 021209c t4 c1

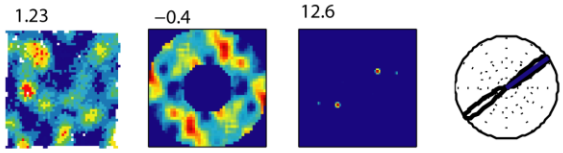

r1682 021209c t4 c2

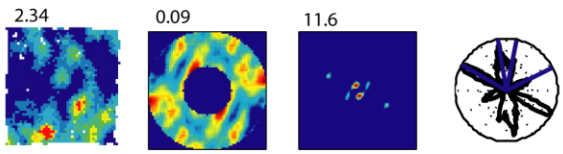

r1682 041209c t4 c1

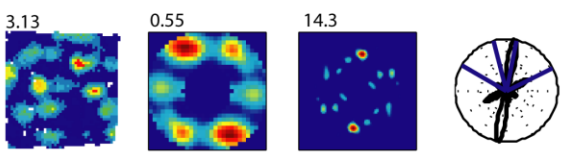

r1682 041209c t4 c3

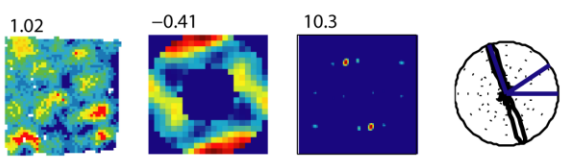

r1738 290710b t1 c1

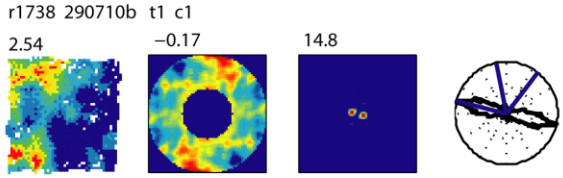

r1738 010810d t1 c3

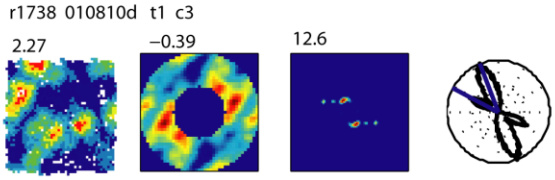

r1738 090810b t1 c1

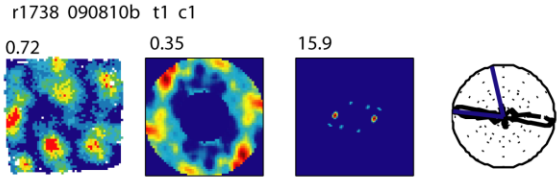

r1738 090810b t1 c3

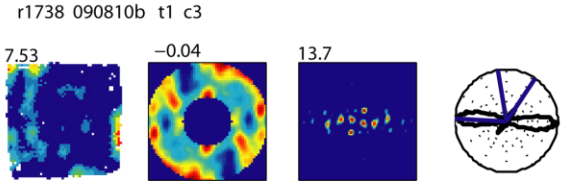

r1738 110810b t1 c1

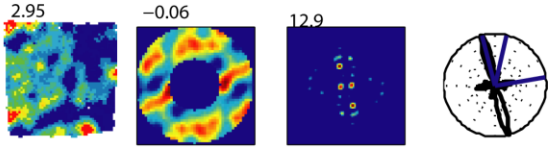

r1738 140810b t1 c4

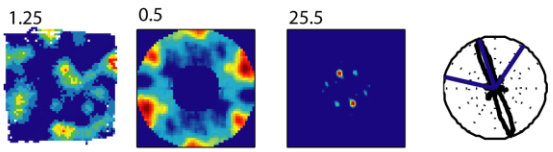

r1738 180810b t1 c1

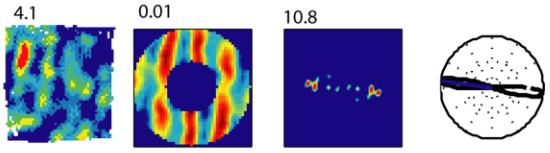

r1738 180810b t1 c3

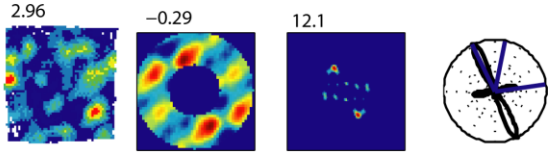

r1738 210810b t1 c2

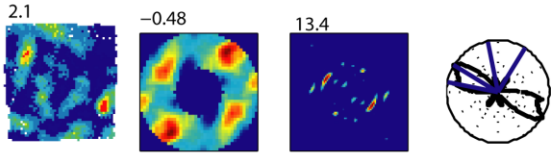

r1738 210810b t1 c1

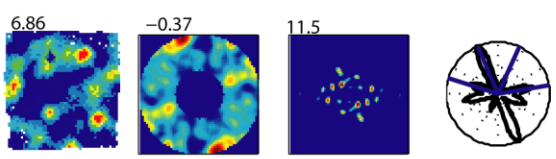

r1738 290710b t2 c1

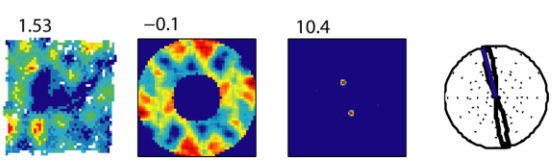

r1738 290710b t2 c5

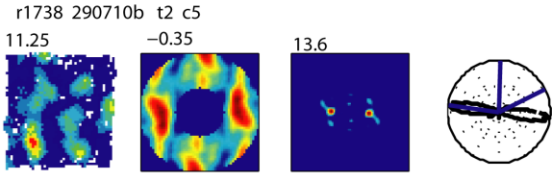

r1738 010810d t2 c5

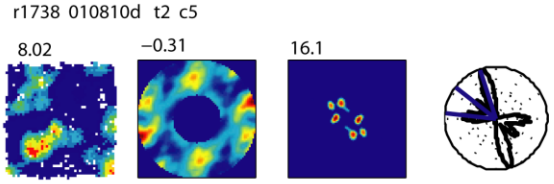

r1738 030810b t2 c1

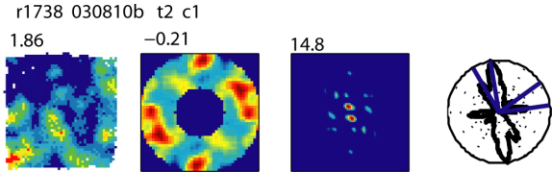

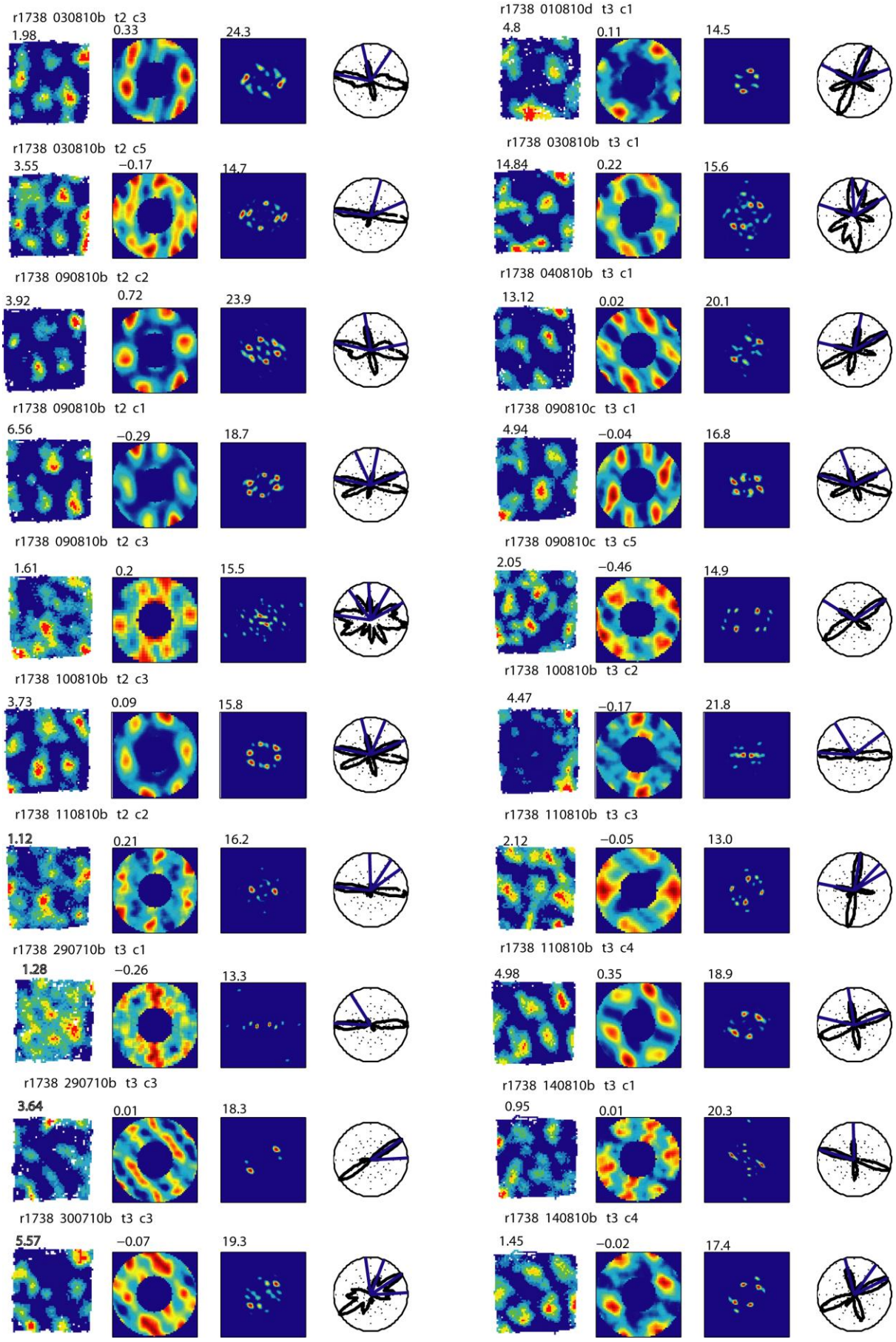
r1738 030810b t2 c3
1.98
0.33
24.3
r1738 030810b t2 c5
3.55
−0.17
14.7
r1738 090810b t2 c2
3.92
0.72
23.9
r1738 090810b t2 c1
6.56
−0.29
18.7
r1738 090810b t2 c3
1.61
0.2
15.5
r1738 100810b t2 c3
3.73
0.09
15.8
r1738 110810b t2 c2
1.12
0.21
16.2
r1738 290710b t3 c1
1.28
−0.26
13.3
r1738 290710b t3 c3
3.64
0.01
18.3
r1738 300710b t3 c3
5.57
−0.07
19.3
r1738 010810d t3 c1
4.8
0.11
14.5
r1738 030810b t3 c1
14.84
0.22
15.6
r1738 040810b t3 c1
13.12
0.02
20.1
r1738 090810c t3 c1
4.94
−0.04
16.8
r1738 090810c t3 c5
2.05
−0.46
14.9
r1738 100810b t3 c2
4.47
−0.17
21.8
r1738 110810b t3 c3
2.12
−0.05
13.0
r1738 110810b t3 c4
4.98
0.35
18.9
r1738 140810b t3 c1
0.95
0.01
20.3
r1738 140810b t3 c4
1.45
−0.02
17.4

r1738 180810b t3 c1

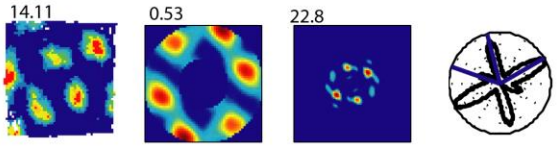

r1738 180810b t3 c4

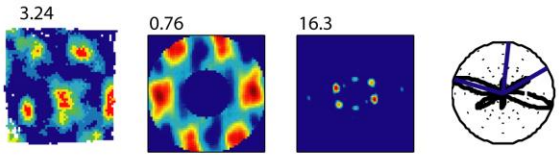

r1738 210810b t3 c3

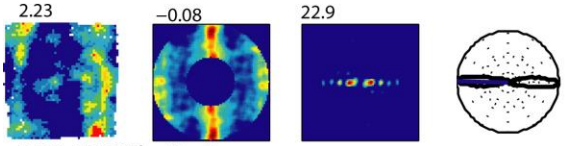

r1738 210810b t3 c4

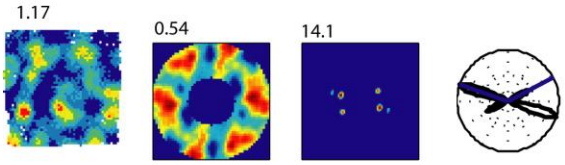

r1738 290710b t4 c1

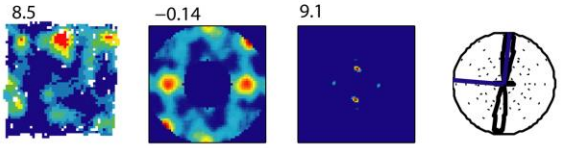

r1738 290710b t4 c2

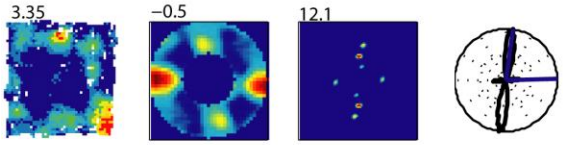

r1738 010810d t4 c2

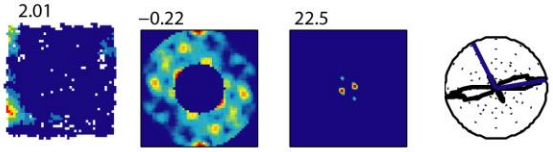

r1738 180810b t4 c4

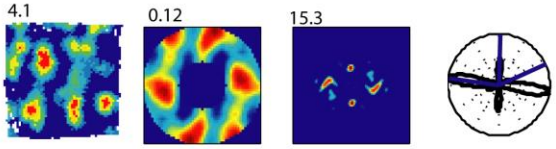

r1738 240810b t4 c1

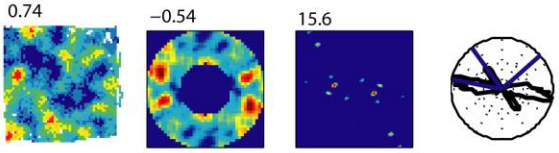

r1709 180210b t1 c1

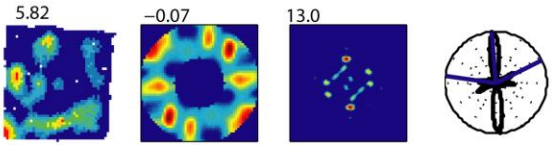

r1709 180210b t1 c2

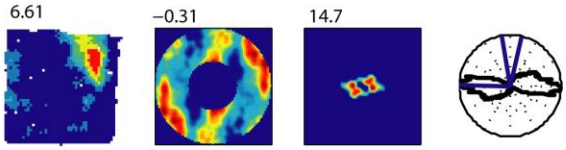

r1709 190210b t1 c1

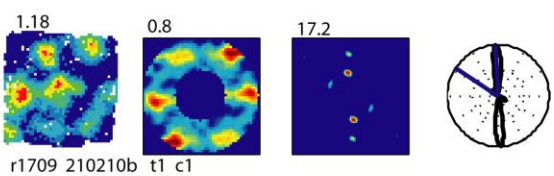

r1709 210210b t1 c1

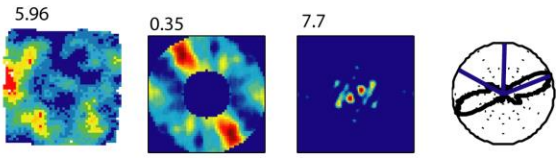

r1709 010310b t1 c1

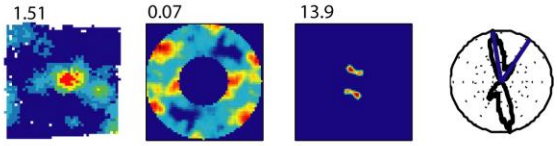

r1709 010310b t1 c5

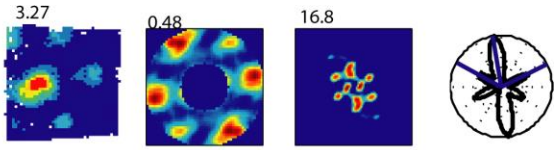

r1709 010310b t1 c6

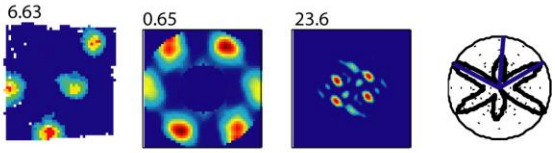

r1709 230210b t2 c1

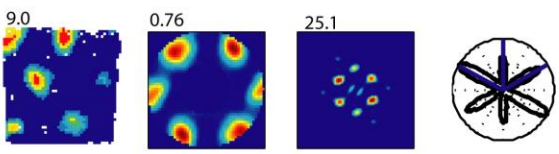

r1709 230210b t2 c3

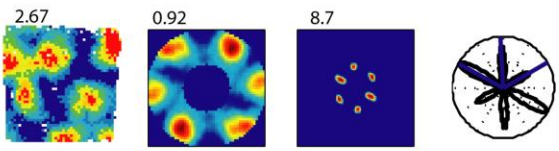

r1709 210210b t3 c1

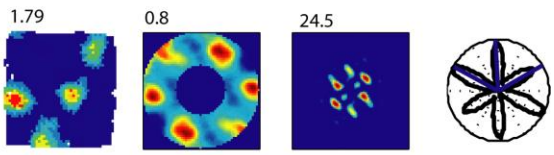

r1709 210210b t3 c3

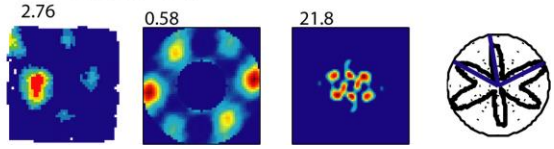

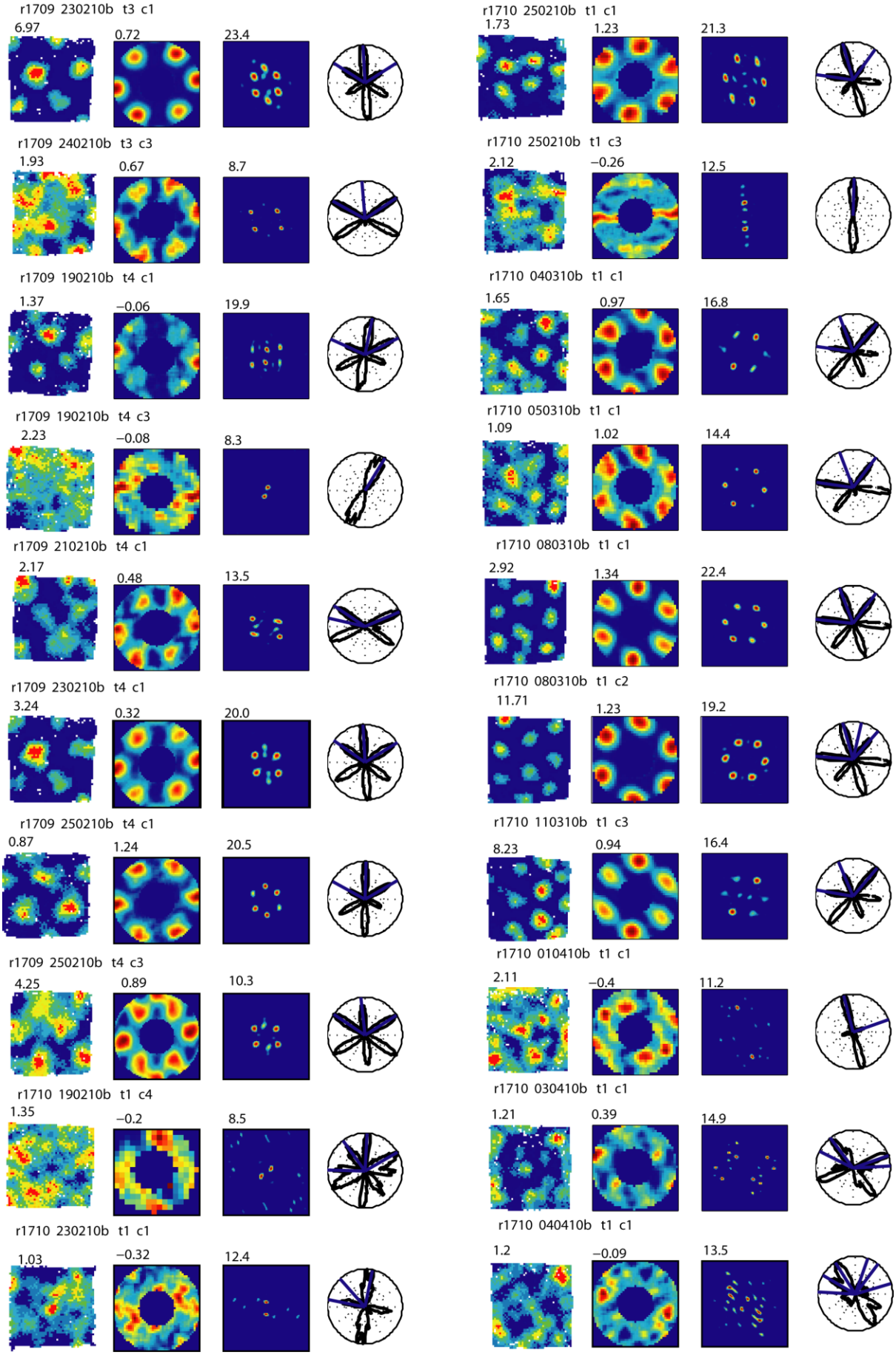
r1709 230210b t3 c1
6.97
0.72
23.4
r1709 240210b t3 c3
1.93
0.67
8.7
r1709 190210b t4 c1
1.37
−0.06
19.9
r1709 190210b t4 c3
2.23
−0.08
8.3
r1709 210210b t4 c1
2.17
0.48
13.5
r1709 230210b t4 c1
3.24
0.32
20.0
r1709 250210b t4 c1
0.87
1.24
20.5
r1709 250210b t4 c3
4.25
0.89
10.3
r1710 190210b t1 c4
1.35
−0.2
8.5
r1710 230210b t1 c1
1.03
−0.32
12.4
r1710 250210b t1 c1
1.73
1.23
21.3
r1710 250210b t1 c3
2.12
−0.26
12.5
r1710 040310b t1 c1
1.65
0.97
16.8
r1710 050310b t1 c1
1.09
1.02
14.4
r1710 080310b t1 c1
2.92
1.34
22.4
r1710 080310b t1 c2
11.71
1.23
19.2
r1710 110310b t1 c3
8.23
0.94
16.4
r1710 010410b t1 c1
2.11
−0.4
11.2
r1710 030410b t1 c1
1.21
0.39
14.9
r1710 040410b t1 c1
1.2
−0.09
13.5

r1710 040410b t1 c3

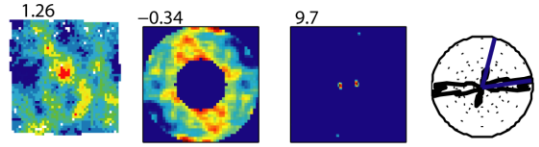

r1710 050410b t1 c3

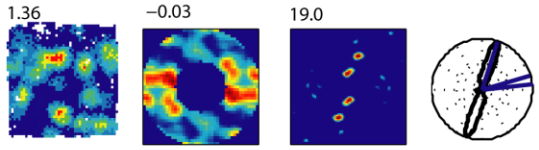

r1710 020310b t2 c1

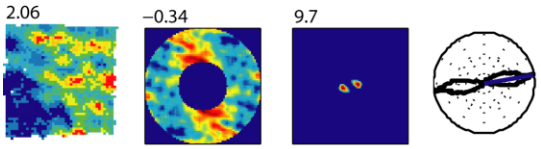

r1710 020310b t2 c3

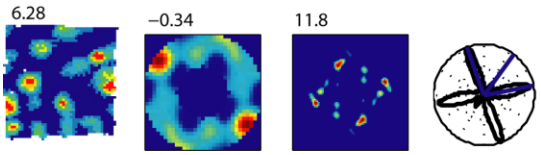

r1710 080310b t2 c1

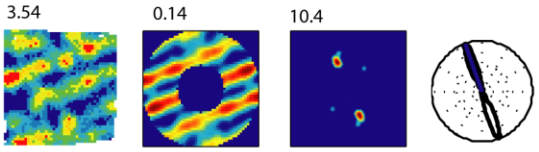

r1710 080310b t2 c3

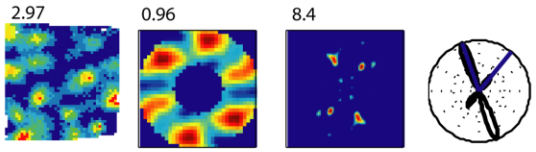

r1710 080310b t2 c4

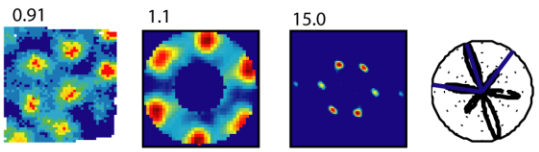

r1710 110310b t2 c4

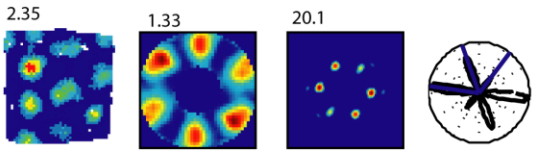

r1710 110310b t2 c5

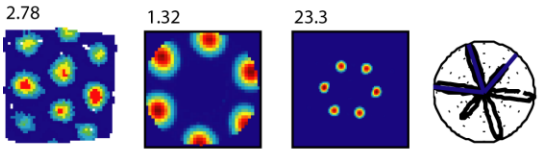

r1710 150310b t2 c1

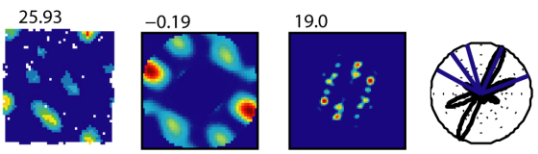

r1710 150310b t2 c3

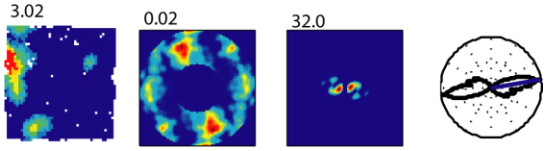

r1710 150310b t2 c5

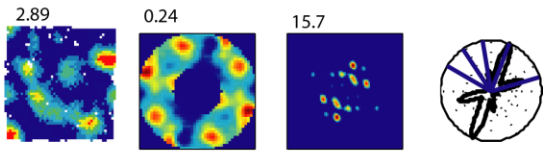

r1710 160310b t2 c1

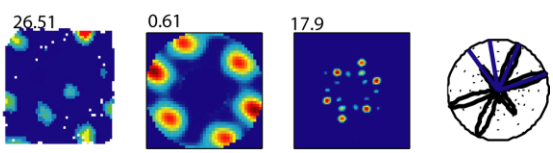

r1710 180310b t2 c1

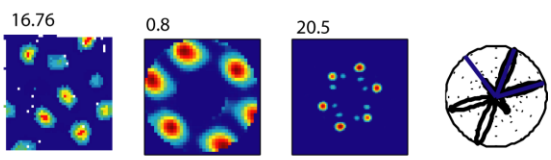

r1710 180310b t2 c3

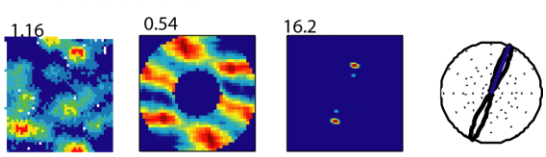

r1710 180310b t2 c4

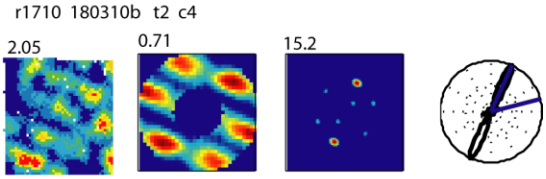

r1710 200310b t2 c3

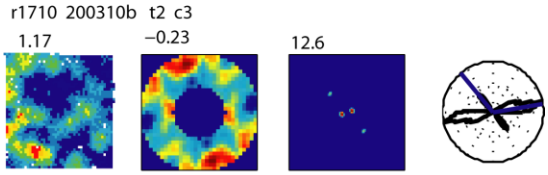

r1710 210310b t2 c1

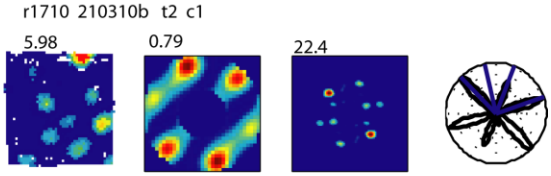

r1710 210310b t2 c3

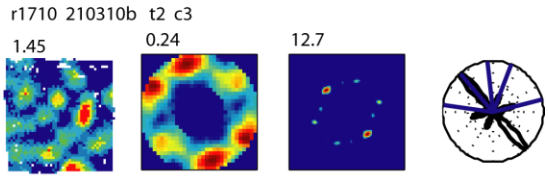

r1710 300310b t2 c1

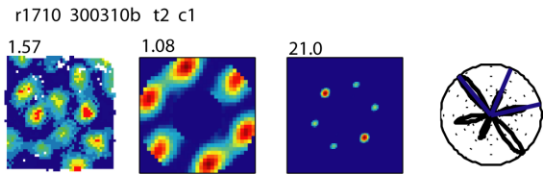

r1710 300310b t2 c4

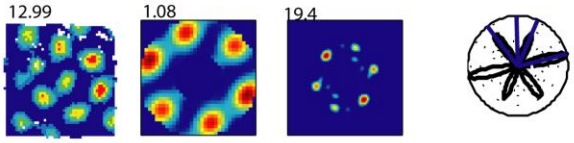

r1710 310310b t2 c3

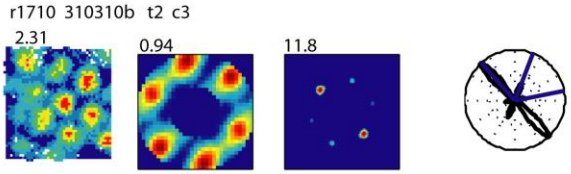

r1710 010410b t2 c1

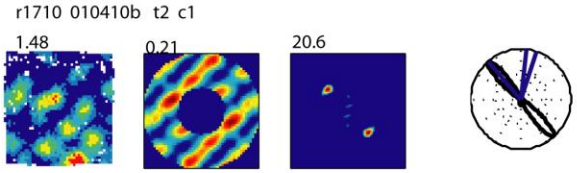

r1710 010410b t2 c4

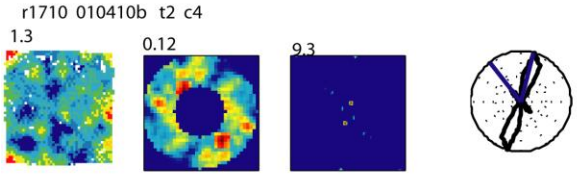

r1710 250210b t3 c3

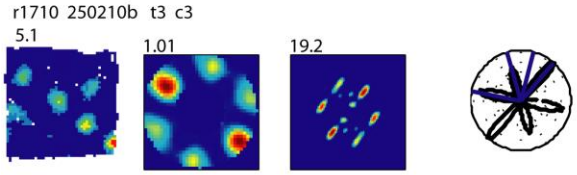

r1710 020310b t3 c1

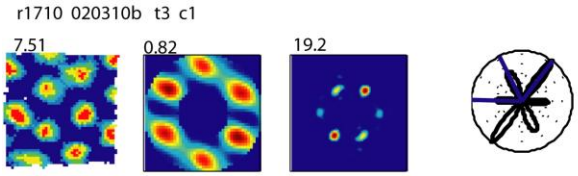

r1710 080310b t3 c3

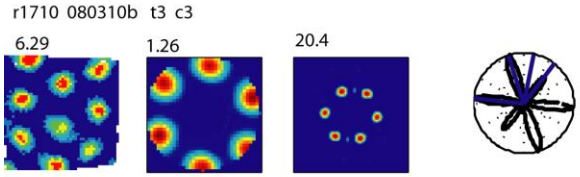

r1710 160310b t3 c1

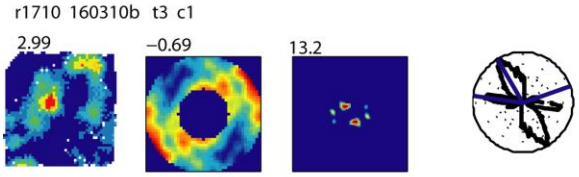

r1710 210310b t3 c1

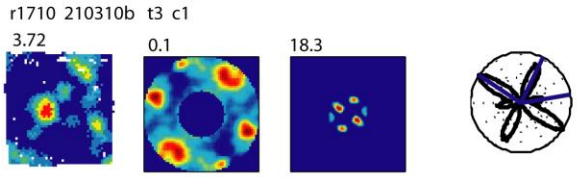

r1710 010410b t3 c1

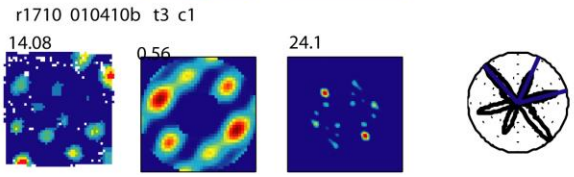

r1710 230210b t4 c1

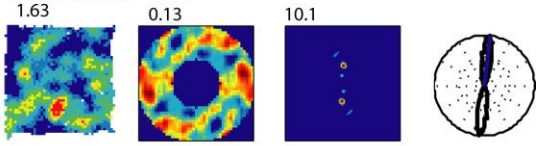

r1710 250210b t4 c1

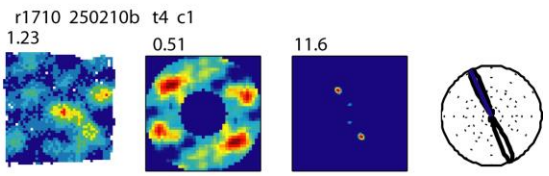

r1710 250210b t4 c3

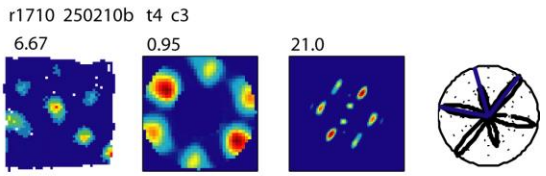

r1710 040310b t4 c1

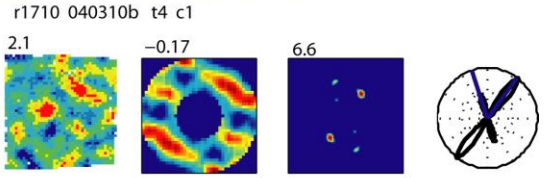

r1710 160310b t4 c3

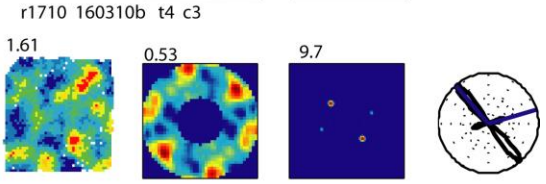

r1710 310310b t4 c4

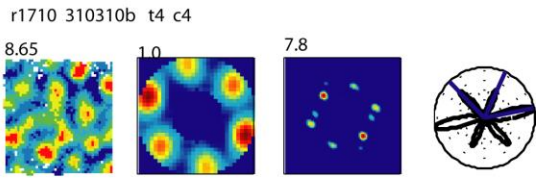

r1710 020410b t4 c1

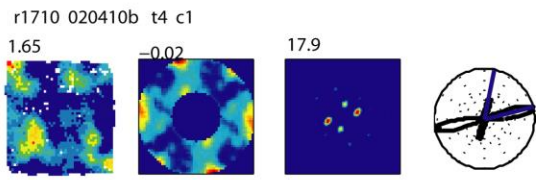

r1728 280410b t1 c3

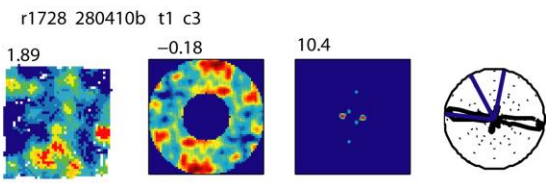

r1728 280410b t3 c1

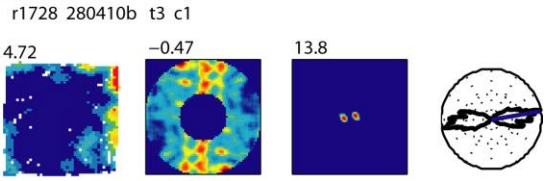

r1728 280410b t3 c2

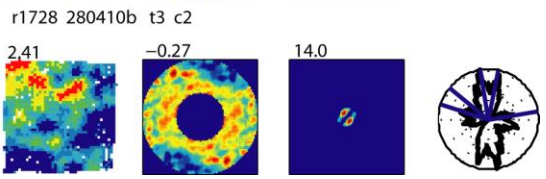

r1728 280410b t3 c3

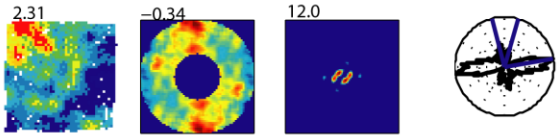

r1728 280410b t4 c1

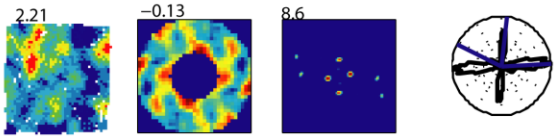

r1728 280410b t4 c2

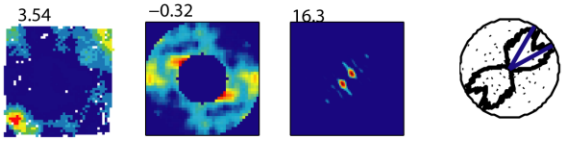

r1728 280410b t4 c3

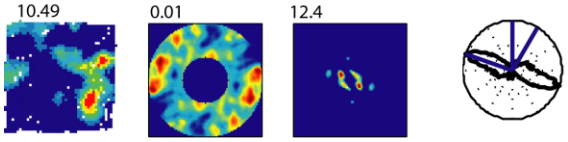

r1728 280410b t4 c4

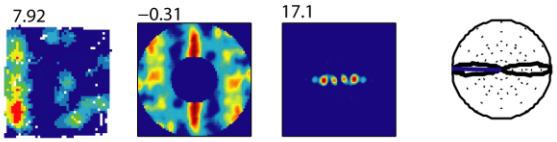

r1728 300410b t4 c4

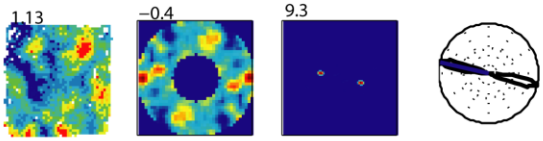

r1728 300410b t4 c5

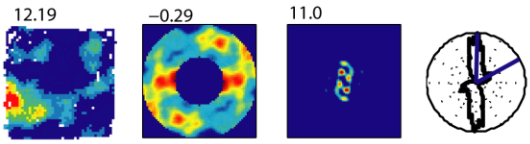

r1728 300410b t4 c7

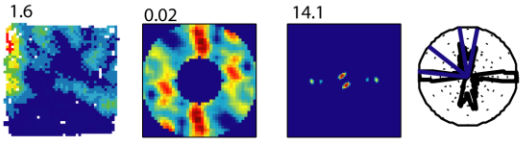

r1728 300410b t4 c8

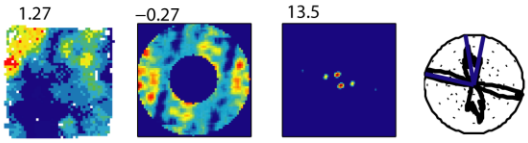

r1728 040510b t4 c3

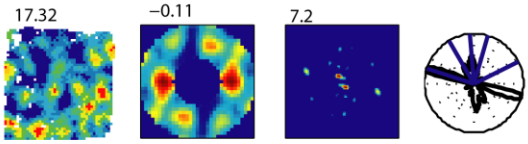

r1728 060510b t4 c1

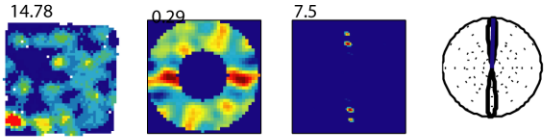

r1728 300410b t3 c1

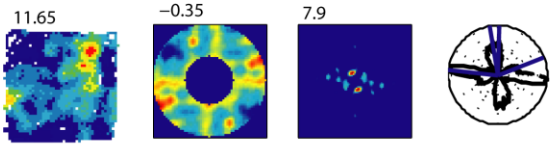

r1728 300410b t3 c3

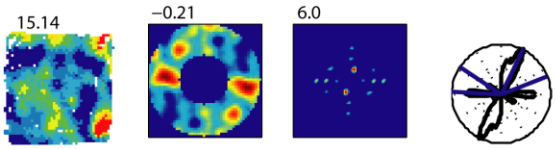

r1728 040510b t3 c1

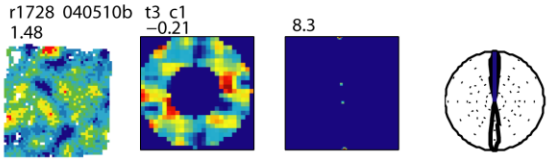

r1728 060510b t3 c1

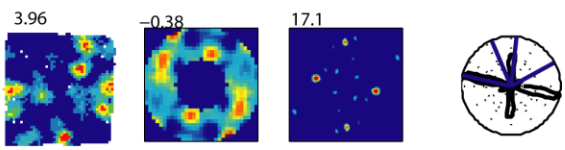

r1728 060510b t3 c7

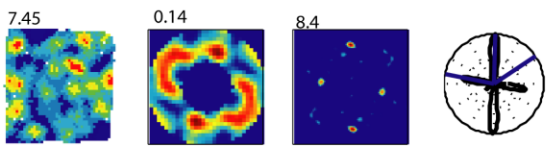

r1728 150510b t3 c1

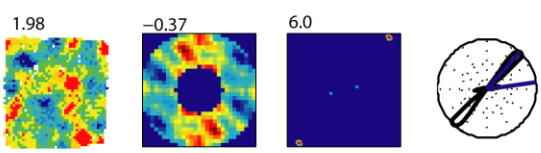

r1728 300410b t2 c1

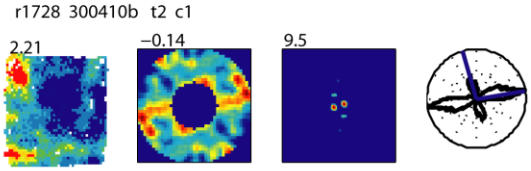

r1728 300410b t2 c5

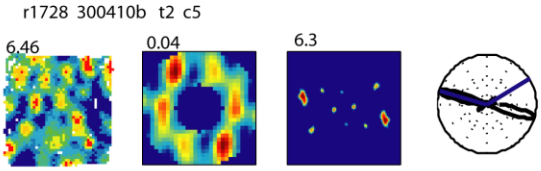

r1728 040510b t2 c1

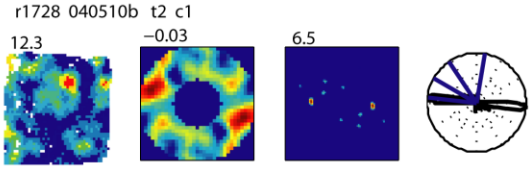

r1728 040510b t2 c3

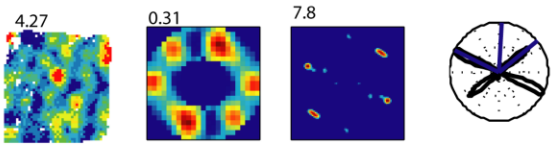

r1728 040510b t2 c4

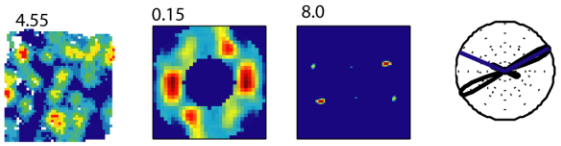

r1728 060510b t2 c1

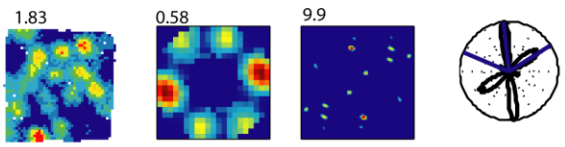

r1728 100510b t2 c1

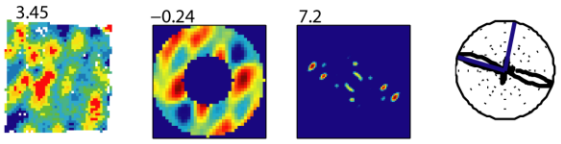

r1728 110510b t2 c3

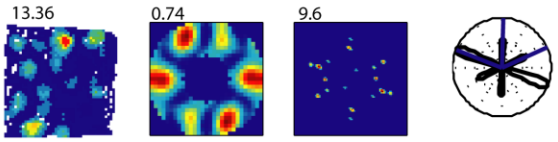

r1728 110510b t2 c4

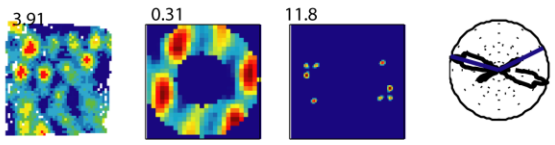

r1728 110510b t2 c6

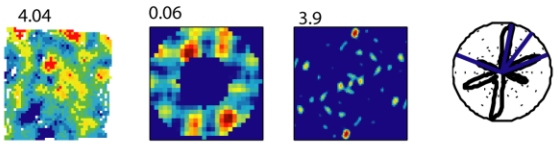

r1728 110510b t2 c7

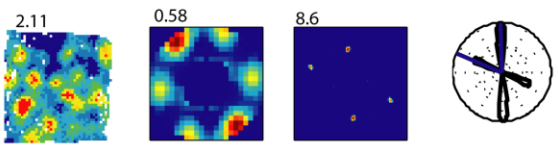

r1728 110510b t2 c8

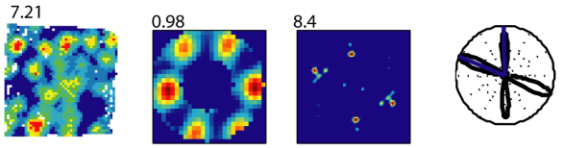

r1728 120510b t2 c1

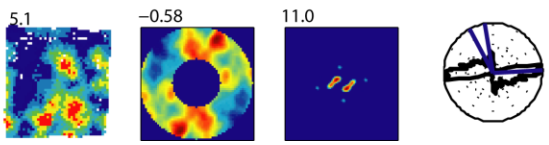

r1728 120510b t2 c4

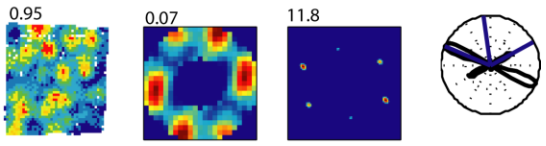

r1728 140510b t2 c1

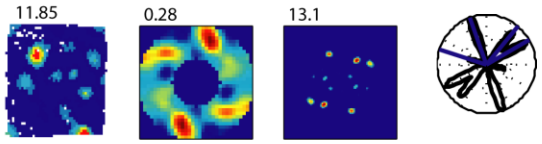

r1728 140510c t2 c4

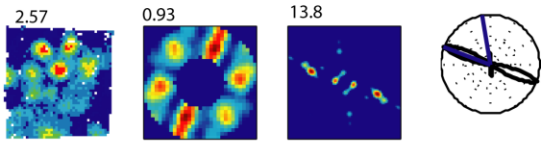

r1728 150510b t2 c1

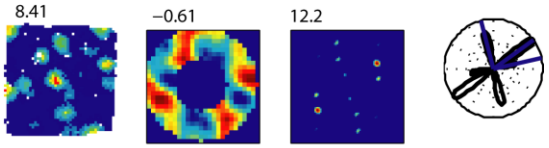

r1728 150510c t2 c3

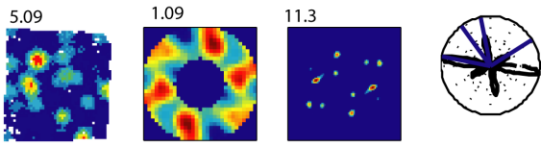

r1728 170510b t2 c1

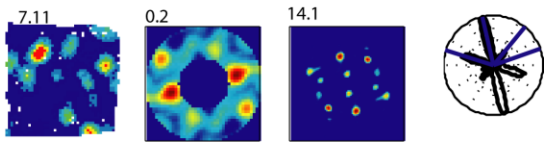

r1728 180510b t2 c2

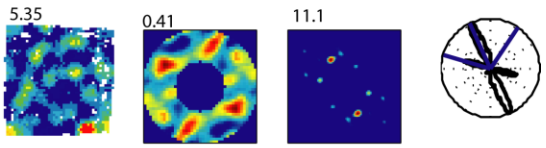

r1728 040510b t1 c1

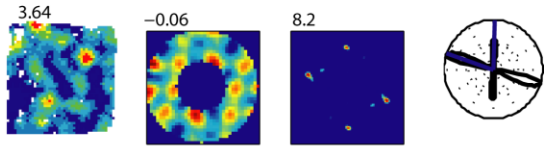

r1728 040510b t1 c4

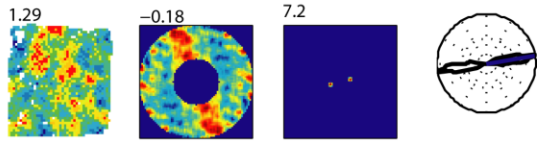

r1728 060510b t1 c1

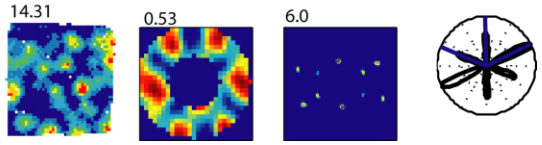

r1728 060510b t1 c3

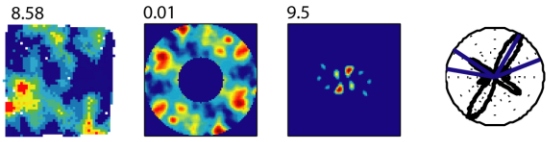

r1728 060510b t1 c4

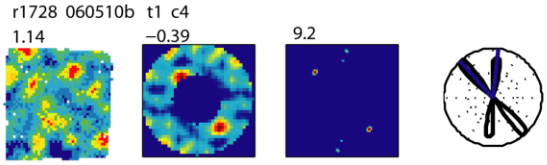

r1728 100510b t1 c2

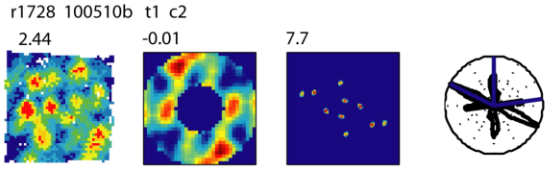

r1728 110510b t1 c1

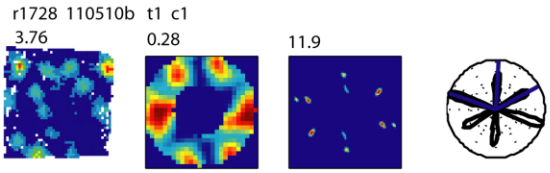

r1728 110510b t1 c3

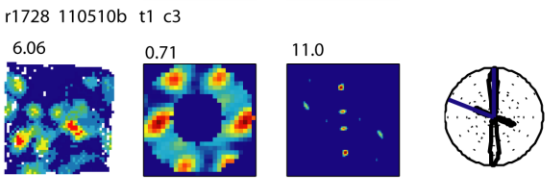

r1728 120510b t1 c1

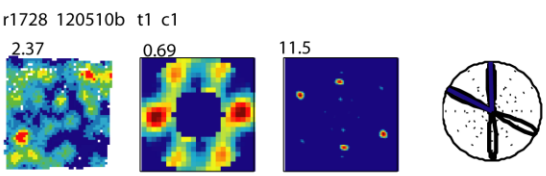

r1728 120510b t1 c2

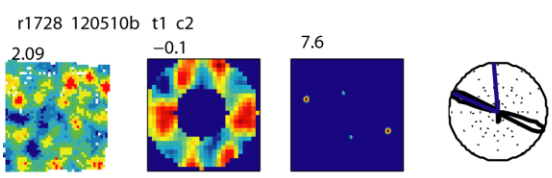

r1728 120510b t1 c3

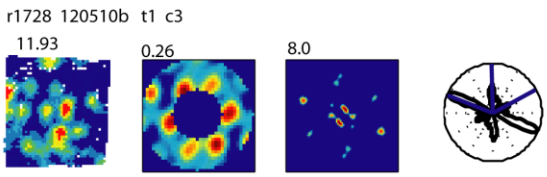

r1728 140510b t1 c1

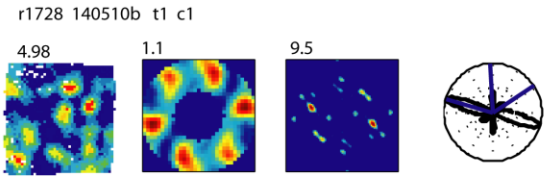

r1728 140510b t1 c3

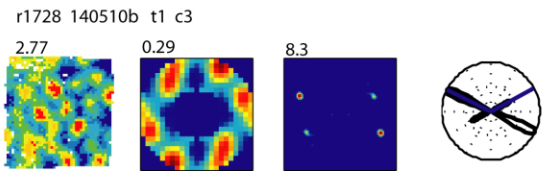

r1728 140510b t1 c4

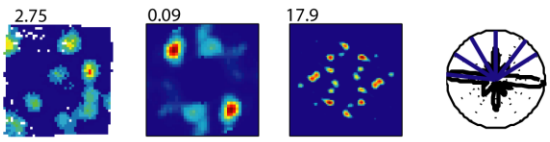

r1728 140510c t1 c5

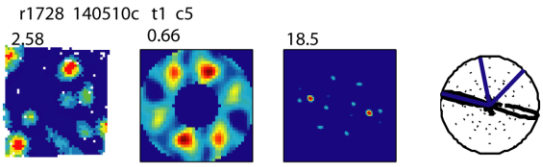

r1728 140510c t1 c6

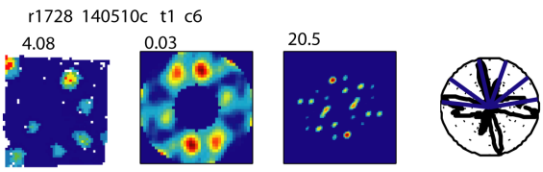

r1728 150510c t1 c2

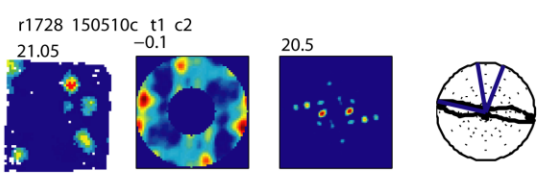

r1728 150510b t1 c3

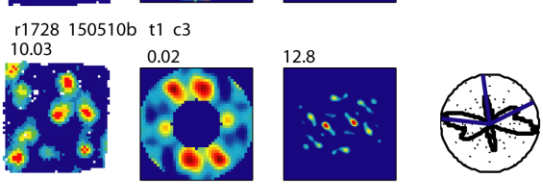

r1728 170510b t1 c1

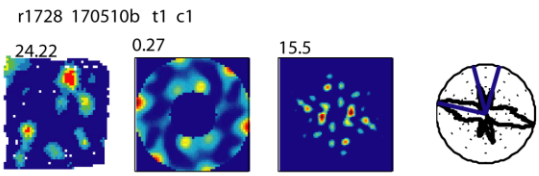

r1728 170510c t1 c1

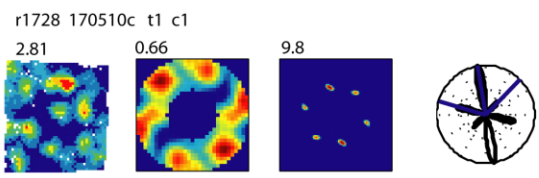

r1737 280610b t1 c1

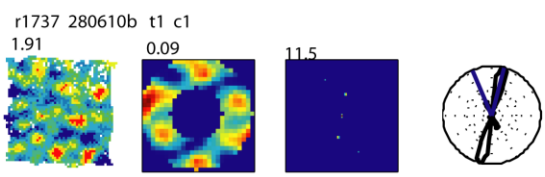

r1737 280610b t1 c3

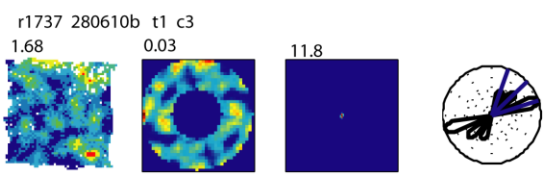

r1737 290610b t1 c1

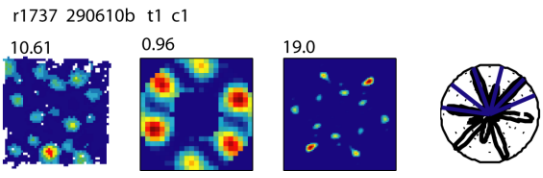

r1737 060710b t1 c4

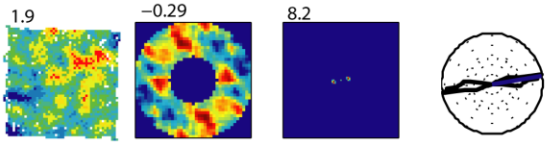

r1737 210710b t1 c3

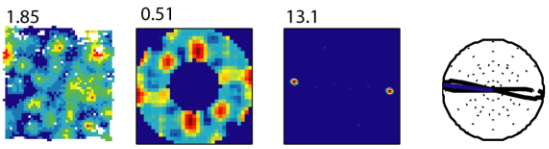

r1737 210710b t1 c4

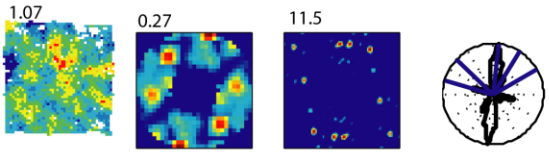

r1737 240710b t1 c1

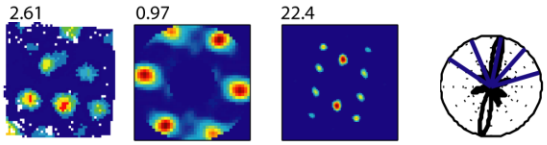

r1737 240710b t1 c3

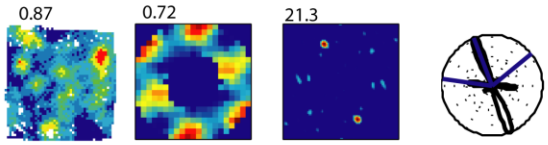

r1737 260710b t1 c3

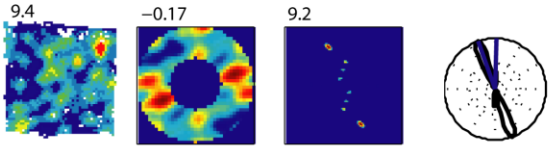

r1737 280710b t1 c3

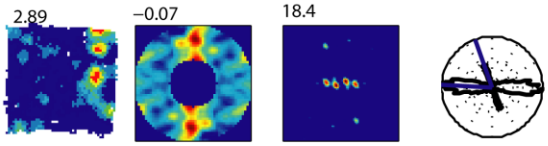

r1737 280710b t1 c5

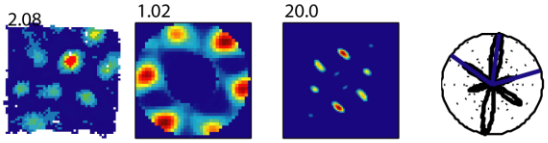

r1737 290610b t2 c1

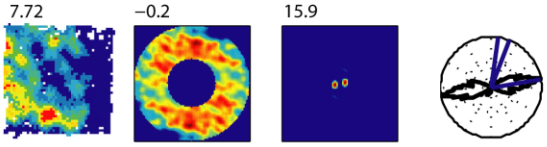

r1737 030710b t2 c3

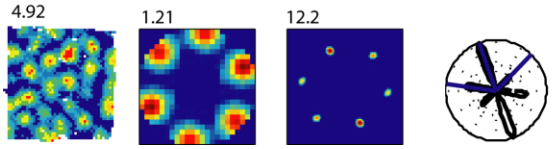

r1737 290610b t3 c1

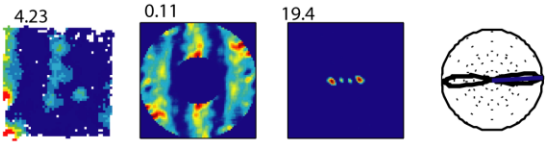

r1737 290610b t3 c3

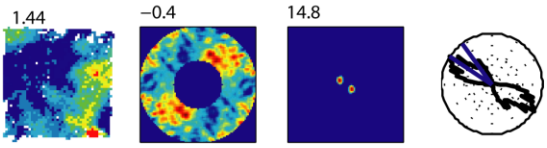

r1737 030710b t3 c3

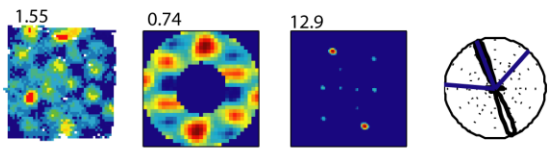

r1737 050710b t3 c1

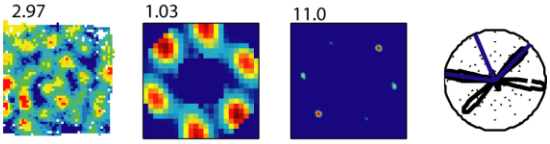

r1737 050710b t3 c3

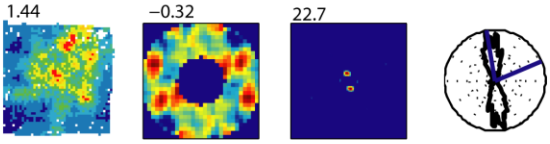

r1737 060710b t3 c1

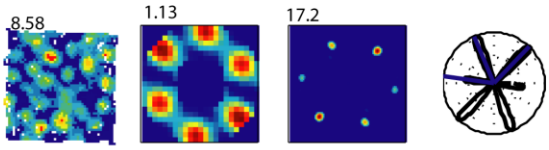

r1737 210710b t3 c3

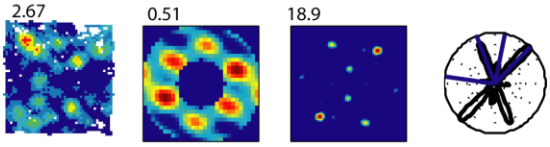

r1737 290610b t4 c1

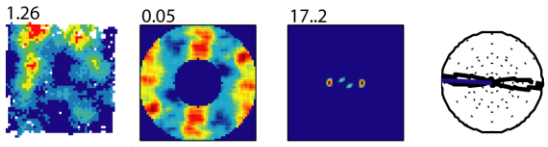

r1737 030710b t4 c1

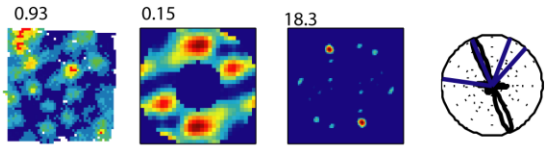

r1739 020810b t2 c1

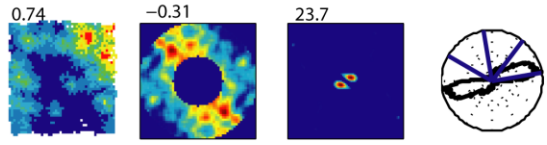

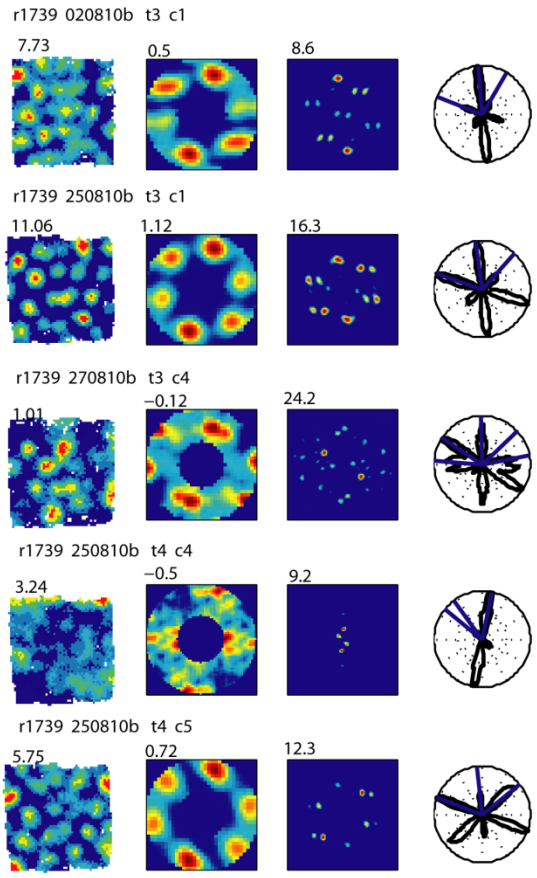

Fig. S15. The rate maps, spatial autocorrelograms, two dimensional Fourier spectrograms and Fourier polar plots of all the spatially periodic cells with their peak firing rate, gridness score and maximum Fourier power indicated on the top left corner of the rate maps, spatial autocorrelograms, two dimensional Fourier spectrograms respectively.

	Same environment	Different environment
No change occurred	40 cells (89%, N=45)	19 cells (68%, N=28)
Change occurred	5 cells (11%, N=45)	9 cells (32%, N=28)

Table S1. The frequency of changes in spatially periodic firing between grid and non-grid patterns in the same (1 m circle or 1.3 m square) enclosure and across different environments (from 1 m circle to 1.3 m square enclosure). The 9/28 cells showing a change between environments is significantly above that expected from the spontaneous rate of change in the same environment (11%), p=0.002 (binomial test).